Title
Guiding Cell Behavior in 2D, 3D, and Dynamic Environments

Author
Mercurio, Kevin

Publication Date
2013

Peer reviewed|Thesis/dissertation

Guiding Cell Behavior in 2D, 3D, and Dynamic Environments

by

Kevin Mercurio

A thesis submitted in partial satisfaction of the
requirements for the degree of Master of Science in

Biological Engineering and Small-scale Technologies

University of California at Merced – School of Engineering

Committee in charge
Dr. Valerie Leppert, Chair
Dr. Kara McCloskey
Dr. Chunchih Tung

Fall 2013

The thesis of Kevin Mercurio is approved, and is acceptable in quality and form for publication on microfilm and electronically:

Dr. Valerie Leppert, Chair

Date

Dr. Kara McCloskey

Date

Dr. Chunchih Tung

Date

University of California, Merced

2013

Acknowledgements

First and foremost, I would like to acknowledge my advisor Dr. Valerie Leppert. I am grateful for the opportunity she gave to me to become a researcher in the materials science laboratory at the University of California at Merced. Thanks to her, I gained valuable hands-on experience in the lab with advanced equipment like the Electron Microscopes and got the opportunity to attend conferences for the Materials Research Society in San Francisco, CA.

In addition, I would like to thank each of the graduate students from the Leppert group: Kennedy Nguyen, Gayatri Premasekharan, and Aaron Cowles, for their positive feedback and constructive criticism. I also thank undergraduate students Jacob Petersen, Ian Donahue, Heather Jackson, David Magginetti, Ariel Parker, and Michael Urner for providing feedback on my writing.

Moreover, I thank and acknowledge Dr. Kara McCloskey for allowing me the opportunity to work on research projects in her lab space. I also appreciate her feedback and support on the many posters, papers, and presentations I prepared. In collaboration with the McCloskey lab, I express thanks to all of the postdoc, graduate, and undergraduate students who helped me in the lab with cell culture experiments, including Dr. William Turner, Jesus Luna, Drew Glacier, Andrew Burns, Robby Puccinelli, Lian Wong, Nabjot Sandhu, and the rest of the group.

Furthermore, I would like to thank other individuals who have made a large impact on my education and who have helped me advance my research projects in one way or

another. I thank Dr. Christopher Viney for his discussions on polymers and his critiques on my writing. I thank Dr. Lillian Davila for her support and feedback on my research topic and also her flexibility and willingness to review my work. I thank graduate students Yang Liu and Jose Flores for helping me with AFM characterization in Jennifer Lu's lab space. I also thank Venu Polini for his help using the Confocal Microscope in the SCIF workspace. Lastly I want to express gratitude to Mike Dunlap and the Imaging Microscopy Facility at UC Merced. Mike seemed to always know a solution or answer to solving difficult issues and fixing equipment.

I want to thank and recognize the funding sources that helped contribute to this research project. This work was performed under the auspices of the NSF (COINS) by University of California Merced under contract number 0832819.

Table of Contents

List of Figures

Abstract

Cell culture substrates for contact guidance studies can be developed through polymer processing to produce various topographic dimensions. Surface topography has a large influence on cell fate and can ultimately be used to help understand and direct cell behaviors. Fabrication techniques for nano- and micro-patterning are typically costly and require large, laboratory-grade equipment. However, in the past decade, researchers have discovered shrink-based techniques to produce nano-scale topography at a fraction of the cost. The fabrication methods are simple, fast, and cost effective, when compared to lithography-based patterning methods. 2D topography is developed using a lab-on-a-chip approach, in which pre-strained polystyrene sheets are coated with metal, constrained from the edges, and heat-treated to develop 320nm and 510nm surface wrinkles. An increase in metal coating thickness from 15nm to 60nm resulted in an increase in wrinkle width and height. To build upon this phenomenon, the polystyrene sheets were further manipulated to generate 3D topography. Acetone solvent was used to craze the polymer sheet and develop surface topography on the micro-scale. Depending on sheet orientation and treatment procedure, wrinkles, channels, and voids ranging in width from 1 μm to 210 μm can be produced. These patterned sheets were then used to mold polydimethylsiloxane (PDMS) cell culture platforms. Biological analysis showed good cellular adhesion of human umbilical vein endothelial cells (HUVECs) on the structures surface. Cellular orientation and actin fiber elongation were analyzed on flat controls, nano-scale wrinkles, crazed topography, and

shrunk-crazed PDMS substrates after 24 hours of culture using optical microscopy. HUVECs on the acetone crazed topographies extended the actin filaments roughly 23 μm in length as compared to the flat control having an average length of 51 μm. The shrunk-crazed topography produced better cellular alignment than the crazed topography. Longitudinal and transverse shrunk samples produced cell alignment of about 10 ± 9°and 8 ± 7° from the underlying pattern direction, respectively. In addition to cell analysis on open faced surfaces, cells were also cultured in 3D microchanneled structures to demonstrate the guidance of cells in a dynamically rotating environment. Cells were loaded into PDMS tubular networks and rotated at approximately 1 rotation per hour. As a result, human umbilical vein endothelial cells (HUVECs) and rat aortic smooth muscle cells (RAOSMCs) were able to adhere to the inner surfaces of the channel and confluent layers were formed circumferentially. The use and application for the structures and devices discussed herein are analyzed and evaluated in three separate projects for their potential in bioengineering and tissue engineering applications.

Chapter 1: Introduction

1.1 The Importance of Cells on Substrates

Controlling a cell's shape, morphology, orientation, and alignment are critical aspects in biology and tissue engineering. The alignment of cells can be an indication for the direction of cell division, which can ultimately benefit or limit tissue healing. If cells are unable to connect with one another to promote regeneration, the healing process may be prolonged and inefficient. In bioengineering, we strive to increase the performance of medical care and reduce the time needed for recovery. Therefore, analyzing these aspects in research can help lead to alternative approaches to improving medical procedures and, in the long run, benefit quality of life.

The environment in which the cells are cultured can play a critical role in the overall viability of tissue patches and grafts. Cells that are directly injected into damaged tissues tend to be lost to the surrounding regions, neglecting the damaged zone and preventing healing [1]. Matrix like materials are typically used to help control the transport of cells to desired regions, which can help guide cellular growth and even provide structural support. Matrix materials such as the urinary bladder matrix (UBM), are thin and porous, and allow cells to fill the void spaces over time and recombine with the surrounding tissue to form a confluent layer. However, the UBM has its limitations as well. Characterization of the UBM material shows random morphology and topography [2], which can ultimately limit pathways for cell growth, reducing the cell-to-cell connections needed for communication and regeneration. As a result, this creates

opportunity to create alternative engineering solutions for designing scaffold structures that fully integrate cells with the surrounding structures.

In addition, tissue damage may be worse than what is presented on the surface, which may require implantation of biological tissues to replace injured regions. For example, damaged veins, capillaries, and vasculature in the body can prevent oxygen, blood, and nutrition flow to vital organs. Endothelial cells play an important role in passing blood throughout vascular networks and their viability is critical to human life. The culture of endothelial cells is well documented in the literature; however, culture in 3D environments has repeatedly been a fundamental challenge. Specifically, the cell seeding process does not typically benefit 3D architectural designs, such as circular channels. Normally the channels would be physically rotated by the user in order to guide cells to other regions on the construct; however, this process is inconsistent. The inconsistency lies within the operation and handling of the researcher. In example, the user may apply forces through physical handling of the polymer microchannels or even the operation of utensils may create strains on the microchannel material, which may cause damage to cell types in the channels during each rotation. Therefore, there is a need to improve the cell seeding processes for 3D structures to allow consistency in the production of confluent cell layers and fabrication of in-vitro vasculature for bioengineering applications.

Many researchers have solved challenges similar to these using a variety of nano- and micro-engineering approaches, however, the fabrication techniques are costly, time-consuming, and typically require large-industrial equipment. As a result, we explored

alternative approaches to nano- and micro-fabrication techniques for guiding cellular behavior in 2D, 3D, and dynamically rotating environments.

1.2 Contact Guidance

The extracellular matrix (ECM) is the primary component in tissues that acts as a cellular scaffold [3]. In biology, the ECM naturally contains topographical cues on the micro- and nano-scale in the form of ridges, valleys, channels, and pores [4]. The basement membrane in particular contains topographical features on sub-micron length-scales. Therefore, mimicking in-vivo surfaces may have potential to help researchers in the biomedical and tissue engineering related fields understand the interactions between cells and topographies: a phenomenon known as contact guidance [5]. Contact guidance is a process in biomedical and tissue engineering where cells respond to physical cues upon surface contact to control the cell shape, direction, and orientation of the cells. The interactions between cells and their underlying surface can influence several cell processes, including adhesion, differentiation, migration, proliferation, orientation, cell-to-cell communication and signaling, and regeneration of cells [6].Controlling these processes creates potential to influence biomedical practices and medical devices around the world [7].

When cells are seeded onto flat scaffolds and surfaces, they can spread to great lengths in all directions. However, if the underlying surface is patterned directionally, the cells will follow paths of least resistance when spreading out, instead of crossing edges [8]. Therefore, cells will align and orient themselves in the direction of surface patterning

which can change the connection paths between cells. Cells are considered to be aligned if their long axis is oriented within 20° of the underlying topography [9]. Studies have shown that aligned cells can influence electrophysiological properties and may be of critical importance to vital organs like the heart [10]. Ultimately the absence of alignment can impair the viability of biological structures and can impair the growth and regeneration process in healing tissues.

The chemistry and topology of a substrate can influence a cells behavior [11]. However, the surface chemistry can limit cells from adhering to substrates if hydrophobic surfaces are present. In some cases, surface treatments are necessary to ensure proper cell seeding to substrates and scaffolds for some polymeric materials. In addition, topography designs that do not allow good cell connections may ultimately limit confluent cell layers and can even cause cell death from the inability to access nutrients. Nevertheless, a number of cell types have been known to respond to surface patterning, including neurons [12], fibroblasts [13], smooth muscle [14], epithelial [15], and endothelial cells [16]. Additionally, control over these cell types can lead to a number of tissue engineering applications including cell sheeting [17], vascular scaffolds [18], and cardiac patches for the heart [19]. Therefore, controlling cell geometry can ultimately affect the function of tissues and organs in living systems.

As mentioned above, there are a number of cell types that can respond to physical cues to change their morphology, alignment, adhesion, and orientation, but the dimensions and shapes of the surface cues can also influence their behavior. In example, research by A. Curtis et al. suggests that shallow grooves below 100nm do not orient the cells

well [20]. Surface features including grooves, steps, wells, and pits can have different effects on cell orientation and adhesion to the substrate [21]. Therefore, the surface features as well as the sizes of those features can ultimately influence the behavior of cells. In addition, many material properties of the substrate can affect cells in contact guidance experiments. For example, studies have shown that material stiffness can have an effect on cell guidance [22]. Moreover, materials used in tissue engineering like polydimethylsiloxane (PDMS) naturally have hydrophobic surfaces and require post-synthesis surface treatments to facilitate cell adhesion [23].

1.3 Conventional Fabrication Techniques

Microfabrication techniques allow the ability to engineer microenvironments for cells and also ultimately control cell geometry and orientation [24]. A number of mainstream micro- and nano-fabrication techniques have been used to produce anisotropic patterning, including abrasion [25], microcontact printing [26], photolithography [27], laser writing [28], electrospinning [29], e-beam lithography [30], and wrinkling techniques [31]. The patterns produced can closely mimic the surfaces of *in vivo* structures, providing realistic dimensions for the analysis of cell types in natural tissues [19]. E-beam lithography and photolithography are widely used methods for their benefit of high resolution and consistent patterning on silicon wafers. Gratings in the nanometer range can be produced using these techniques and may be useful, since cells can react to steps as small as 30 nm [32]. However, these methods are time consuming for both equipment procedure and sample preparation, and are generally expensive

compared to other techniques [33]. To address these issues, we explore low cost and time-sensitive techniques to produce anisotropic patterning and micro-channeled structures for cell guidance.

Chapter 2: Cell Behavior in 2D Environments

2.1 Shrinky Dinks - Pre-strained Polystyrene

Shrinky Dinks plastic sheets are well known for their use as a children's play toy, where designs drawn onto the surface of the sheet can be shrunk to smaller sizes when placed inside an oven. Interestingly, Shrinky Dinks have become a product of particular interest to researchers in recent years for their use in lab-on-a-chip applications and cellular analysis [34]. Shrinky Dinks are thin, transparent, pre-strained polystyrene (PSP) sheets that contract up to 60% in both the x- and y-directions upon heating above their glass transition temperature (T_g) [31]. PSP sheets have shape memory properties, where the polymer can return to a previous shape after having been deformed by heating to the softening temperature of the polymer [35]. During initial processing of the PSP sheets, polystyrene is extruded, rolled into a flat sheet, and then cooled to room temperature. The rolling process induces a large strain into the structure, forcing many of the polymer chains to conform to a flat or 2D position due to the applied compressive stress. This internal stress can thereafter be removed by the addition of an external stimulus, such as thermal energy, causing the polymer to return into its original structure by conforming to the more entropic or random molecular arrangement [36]. As other external forces are applied during the heat-shrinking process, such as an applied strain field, conformational motion may decrease and the overall structure can be restricted to specific dimensions. Thus the physical shape and topographic dimensions can be optimized to different sizes based upon the shrinkage of the sheet and metal coatings.

The ability to shrink PSP sheets for the production of surface patterning provides a fast and inexpensive method for bio-chip production, compared to other techniques mentioned before. Prior literature demonstrates use for microfluidic chips in the fields of biosensing and bioelectronics, where PSP sheets can be tailored for intended use with cells [37]. Researchers also showed that wrinkled topographies, ranging from a few hundred nanometers to several microns in width, can be developed by heat shrinking polymer sheets in-plane using an applied strain field [38]. Others also demonstrate how optimization of the magnitude and direction of applied strain can produce wrinkling patterns of different topographies, generated by the Poisson effect [39].

2.2 Formation of Nano-topography

Traditional techniques for nano-scale fabrication are costly and time-consuming as outlined previously. Researchers C. Fu et al. developed a method for producing nano-topography, based upon research of pre-strained polymer sheets [31]. First, a thin layer of metal (gold) is sputtered onto the surface of the pre-strained polystyrene sheet. Next, the sheet is either constrained by its edges or not constrained, and thereafter heated to induce shrinking of the sheet (Figure 1).

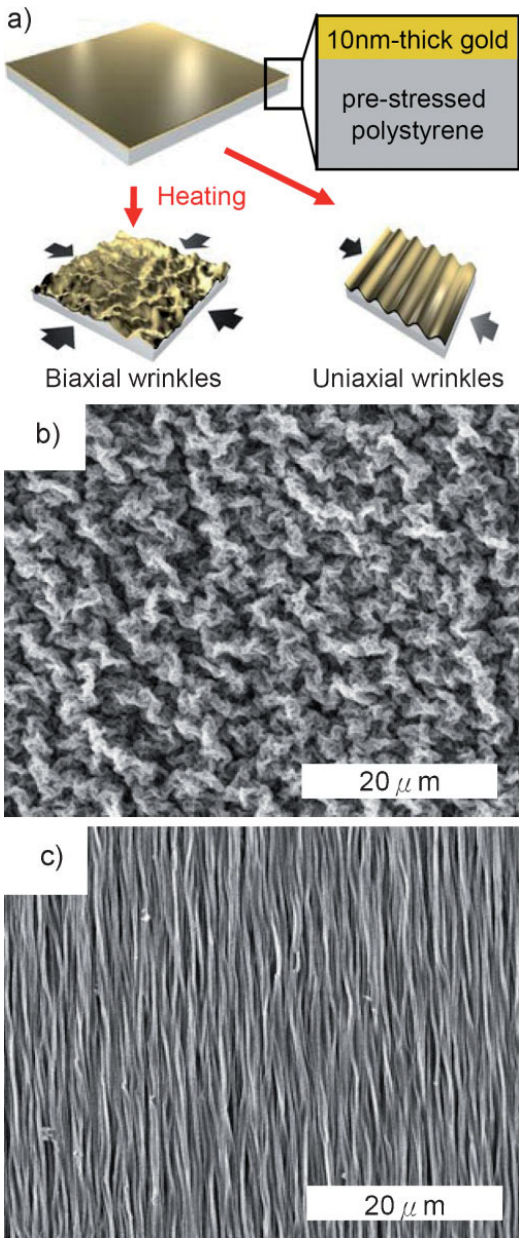

Figure 1: Fabrication of nanowrinkles. a) Scheme of fabrication of biaxial (left) and uniaxial (right) wrinkles. b,c) SEM images of biaxial (b) and uniaxial (c) wrinkles on shrunk polystyrene sheets covered with a 10 nm thick layer of gold [31].

During shrinkage, the soft polymer substrate contracts in-plane due to the residual strain it withholds, however, the stiff metal surface layer cannot contract as the polymer does. As the residual tensile stress in the polymer is released, the metal layer on the surface 'buckles' to form wrinkle morphology. In short, the competition between the elastic bending energy of the stiff metal surface and the elastic energy of deformation of the polymer substrate causes the formation of wrinkling [39]. This wrinkling morphology can be optimized to form different sizes based upon the metal coating thickness. The wrinkling size is directly proportionally related to the Young's moduli of the stiff metal layer and the underlying substrate as well as the metal coating thickness [31].

2.3 Material Results

Following the fabrication methods previously outlined [31], different sizes of anisotropic nanowrinkles were developed by sputtering gold on the surfaces of polystyrene sheets and shrinking them uni-axially. Samples were coated with approximately 10 nm, 20 nm, 30 nm, and 60 nm of gold respectively using a Polaron E5000 sputter coater. This was confirmed by sputtering a glass slide that was masked off and then removing the masking and analyzing the step height with atomic force microscopy (AFM) (Data not shown). An AFM (Park Systems XE-70) was used to analyze the surface dimensions of the wrinkles for each of the samples. Scanning electron microscopy (SEM) and AFM images of the surfaces are seen in Figure 2 below.

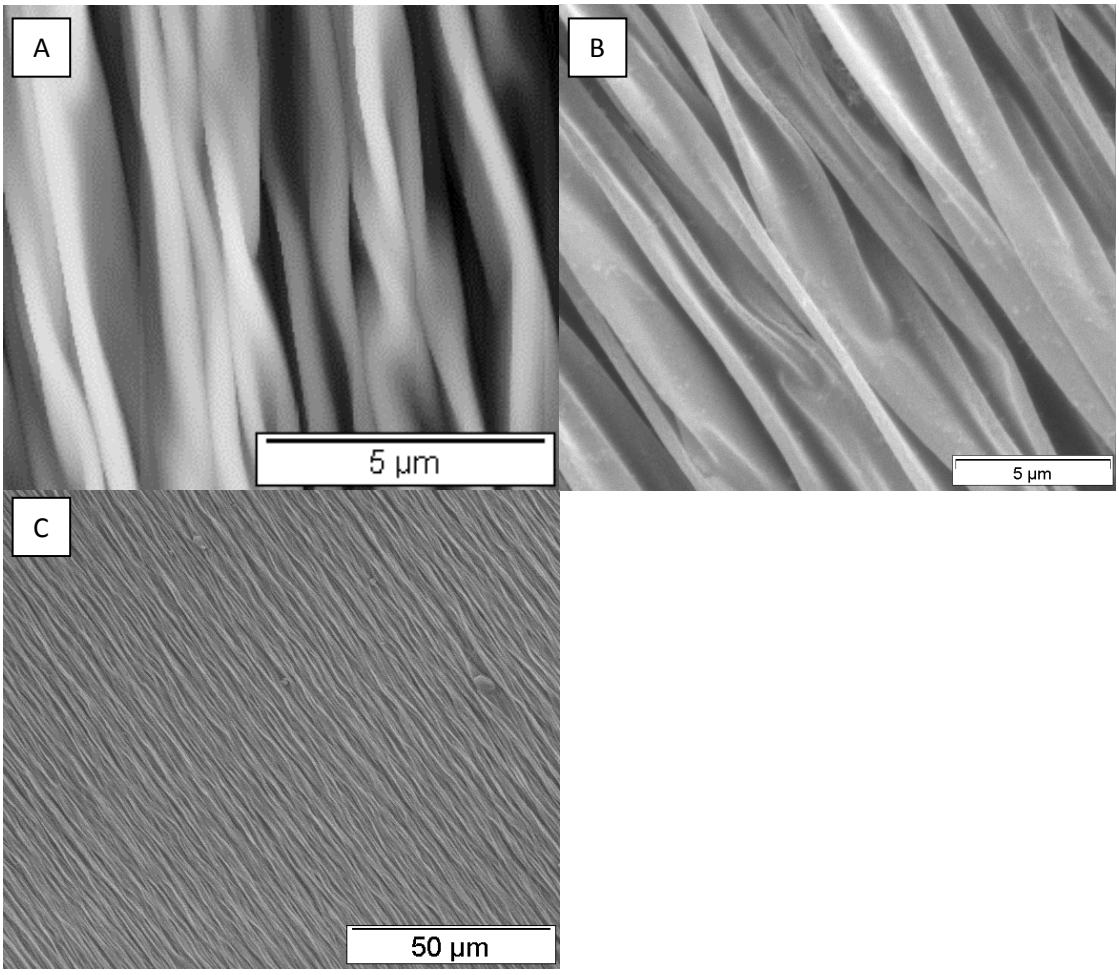

Figure 2: A) AFM image of 15nm gold coated wrinkles B) 30nm gold coated wrinkles and C) SEM low magnification image of (B).

Anisotropic topography was formed following uniaxial shrinking. The results were similar to the work done by C. Fu et al., where an increase in metal layer thickness caused an increase in wrinkle height and also in wrinkle width (Figure 3) [31].

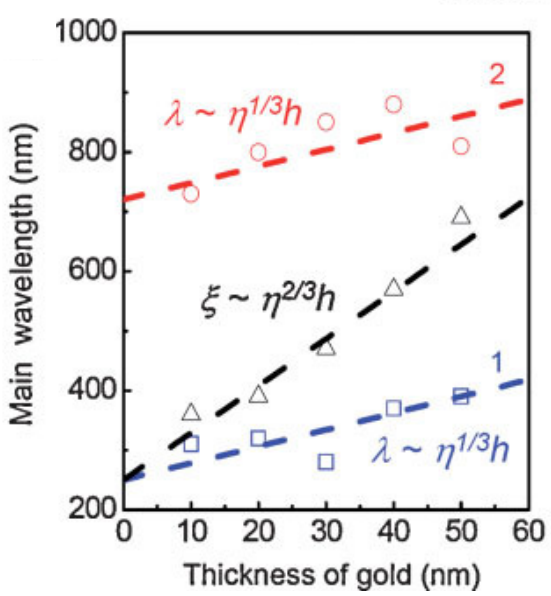

Figure 3: Plot of main wavelength of biaxial (black triangles) and uniaxial (red circles and blue squares) wrinkles as a function of gold layer thickness. The dashed lines show anticipated slopes from the theory [31].

Analysis of the AFM depth profile shows the average wrinkle height increased from 120 nm to approximately 400nm when increasing the gold coating layer from 10 nm to 60 nm respectively (Figure 4).

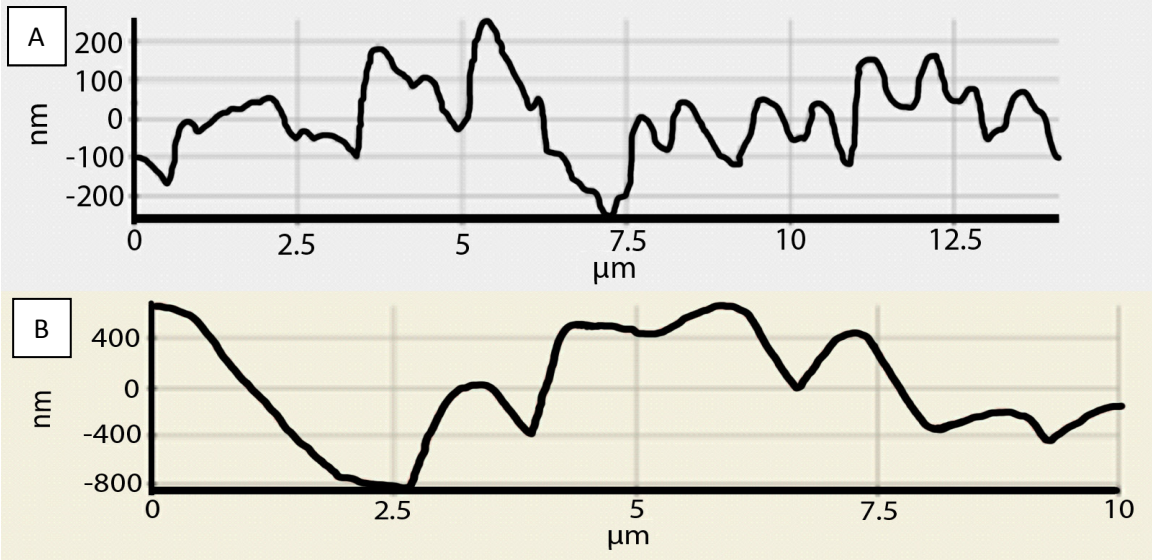

Figure 4: Wrinkle dimension and frequency analysis. A) Wrinkle peak height for 10 nm gold coated sample. B) Wrinkle peak height for 60 nm gold coated sample.

Further analysis showed that the number of wrinkles decreased per unit area as the metal layer thickness was increased. The resulting dimensions are listed below in Table 1 after being analyzed with AnalySIS Pro microscopy software.

Table 1: AFM analysis of wrinkled substrates produced from uni-axial shrinking.

Average Gold Coating (nm)	10	19	30	60
Average Wrinkle Width (nm)	310	430	510	580
Average Wrinkle Height (Crest/Peak to trough) (nm)	120	170	340	400
Approximate Number of Wrinkles per Area (10x10 µm)	30	25	16	12
Wrinkle Uniformity	Uniform	Uniform	Uniform	Non-Uniform

In our analysis, we expected the main wrinkle wavelengths to be closer to the literature values. Characterization in the literature shows that the 10 nm, 20 nm, 30 nm, and 60 nm gold coatings correlate to 300 nm, 320 nm, 280 nm, and 400 nm wavelengths (widths) respectively. In comparison, our results show, on average, a 26% increase in width value. We suspect the large variability between our results is due to the processing conditions, where the heating temperature was raised to 160°C in the literature [31]. The increase in temperature may have caused the first generation of wrinkles to saturate and develop a new set of wrinkles of smaller wavelengths.

2.4 Biological Methods

Polydimethylsiloxane (PDMS) is a widely used elastomer in biological applications due to its inherent properties: transparent for imaging, biocompatible for cell studies, permeable to gas, and ability to be manipulated for molding and soft lithography [40]. Methods for achieving inverse-wrinkling patterns on PDMS were followed from research by Luna et al. where PDMS substrates were cast from the original metallic mold [34]. A detailed figure of the methodology is visualized below in Figure 5.

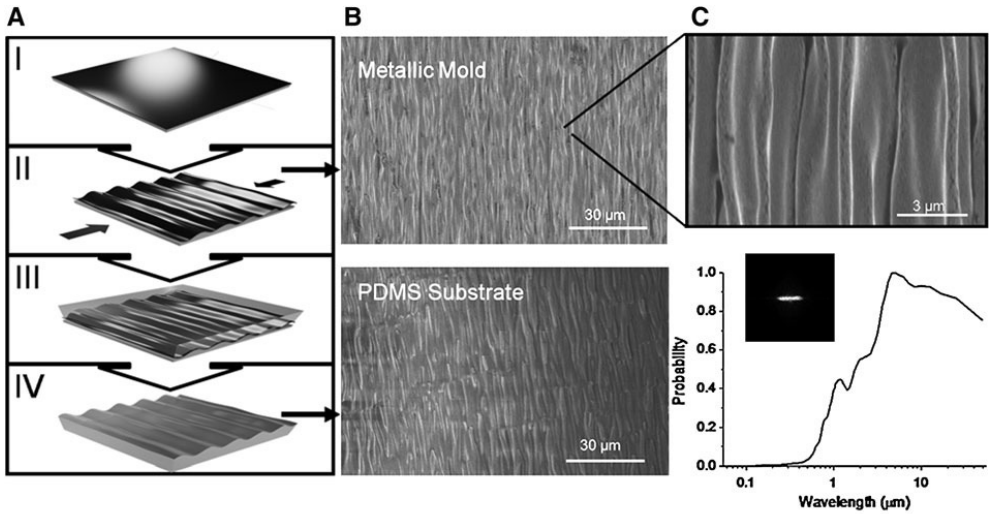

Figure 5: Fabrication and characterization of multi-scale wrinkle substrate. (A) (I) Metallic layer is deposited on PSP sheet. (II) PS is induced to thermally shrink while constrained from opposite sides. (III) The metal wrinkles are used as a soft lithography mold to generate a PDMS substrate (IV), which is used to culture cells. (B) SEM image of of metal wrinkles (with high-resolution inset) and PDMS substrate. (C) The length scale distribution from Fast Fourier transform of SEM images. Inset shows high degree of anisotropy [34].

To determine cellular alignment on the wrinkled substrates, human umbilical vein endothelial cells (HUVECs) (Invitrogen) and rat aortic smooth muscle cells (RAOSMCs) were used. HUVECs were cultured in EGM-2 (Lonza) media for four days from thaw on Corning Tissue Culture 100 mm dishes coated with 0.5% gelatin. HUVECs were seeded onto the chips by the following method: First the EGM-2 media is aspirated and replaced with 10 ml of 1x Phosphate Buffer Solution (PBS), to wash away any

unattached cells or debris, as well as any trypsin neutralizing elements in the media. The PBS was aspirated and 6 ml of 1x trypsin (Invitrogen) was added for 5 minutes while plates were kept at 37°C in an incubator to induce enzymatic cleaving of extracellular proteins. The trypsin was neutralized with an equal amount of media, made of 10% Fetal Bovine Serum (FBS) and 90% PBS. RAOSMCs were treated similarly but using SMGM-2 media (Lonza) instead. Cells were collected into a 15 ml conical tube (Corning), counted and spun at 1200 rpm for 5 minutes. After the supernatant was aspirated, the cells were then re-suspended in media and plated onto the fabricated PDMS chips at a seeding density of 30,000 cells/cm^2 (Prior to plating, the PDMS was charged for a minimum of 15 minutes using an ozone plasma machine (Jelight Company Inc.), and then coated with 0.5% gelatin for 1 hour). Cells were allowed 24 hours to culture on the fabricated substrates, after which the cells were fixed with 4% paraformaldehyde for 15 minutes. To stain the cells, the paraformaldehyde was aspirated and the cells were washed twice with PBS to remove any remaining reagents. Blocking and permeablization solution containing 1% Bovine Serum Albumen (Sigma), 0.7% triton-x (MP Biomedicals), and 6.5% donkey serum was added to the cells and incubated for one hour (3 ml of BSA in PBS at a concentration of 1 mg/ml, 150 µl of donkey serum, and 21 µl of Triton-X 100). After one hour of blocking, 1 µl of Alexa Fluor 488 Phalloidin (Invitrogen) and 5 µL of 2 ng/mL DAPI (CalBiochem) were added to the 500 µl of blocking and permeablizing solution in which the cells are submerged. The cells were left to stain at room temperature for one hour, or alternatively at 4 degrees overnight in a standard refrigerator. Afterwards, the cells were washed twice with PBS and images

were captured using a Nikon Eclipse TE2000-U fluorescence microscope and NIS-Elements AR 3.1 software. Measurements of the cell alignment and elongation were determined using AnalySIS Pro software.

2.5 Biological Result and Impact

Fluorescence microscopy was used to analyze the cells on PDMS mold replicas. At least 100 measurements were recorded for each sample type using the AnalySIS Pro software. The control samples indicated no particular directional alignment or orientation of cells on the flat dish surfaces (Figure 6). Cells created confluent and semi-confluent layers on the polystyrene tissue culture plates.

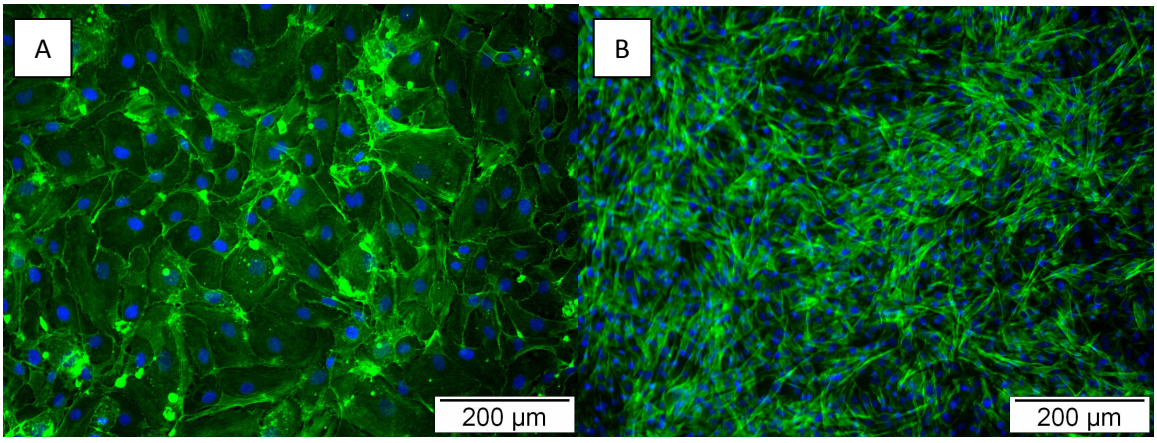

Figure 6: Fluorescence microscopy images of cells on flat polystyrene tissue culture plates. A) HUVECs control and B) RAOSMCs control, captured at 10x magnification.

However, on the 310 nm and 510 nm wrinkles fabricated from 15 nm and 30 nm gold coatings respectively, HUVECs aligned and elongated in the direction of the topography surface (Figure 7A,7B). The cells on the 310 nm wrinkles exhibited greater elongation compared to the 510 nm wrinkles just after 24 hours in culture. However, HUVECs on the 510 nm wrinkles were still significantly aligned and elongated when compared to the control sample. AnalySIS Pro measurements showed that HUVECs on the 310 nm wrinkles, elongated to an average length of 68 ± 26 μm. Approximately 90% of the cells were aligned on the chip on day 3 in culture. HUVECs on the 510 nm wrinkled chip elongated to an average length of 48 ± 18 μm and roughly 84% of the cells were aligned at day 3. HUVECs on the 310nm wrinkles obtained an elongation factor (aspect ratio) greater than the 510 nm wrinkles indicating greater elongation of the actin filaments (data not shown). However, the 510 nm wrinkles also allowed cells to align within 30° of the underlying surface topography direction, so both nano-topographies were consistently beneficial for the alignments and elongations of HUVECs. In addition, RAOSMCs aligned and elongated on the 310 nm wrinkled substrates (Figure 7C). Our analysis showed that roughly 80% of the cells were aligned on the wrinkles within 30° of the underlying topography. The RAOSMC density also decreased by roughly 15% on the 310 nm wrinkles from the original seeding density, possibly due to cells lost to the surrounding media in the tissue culture plate.

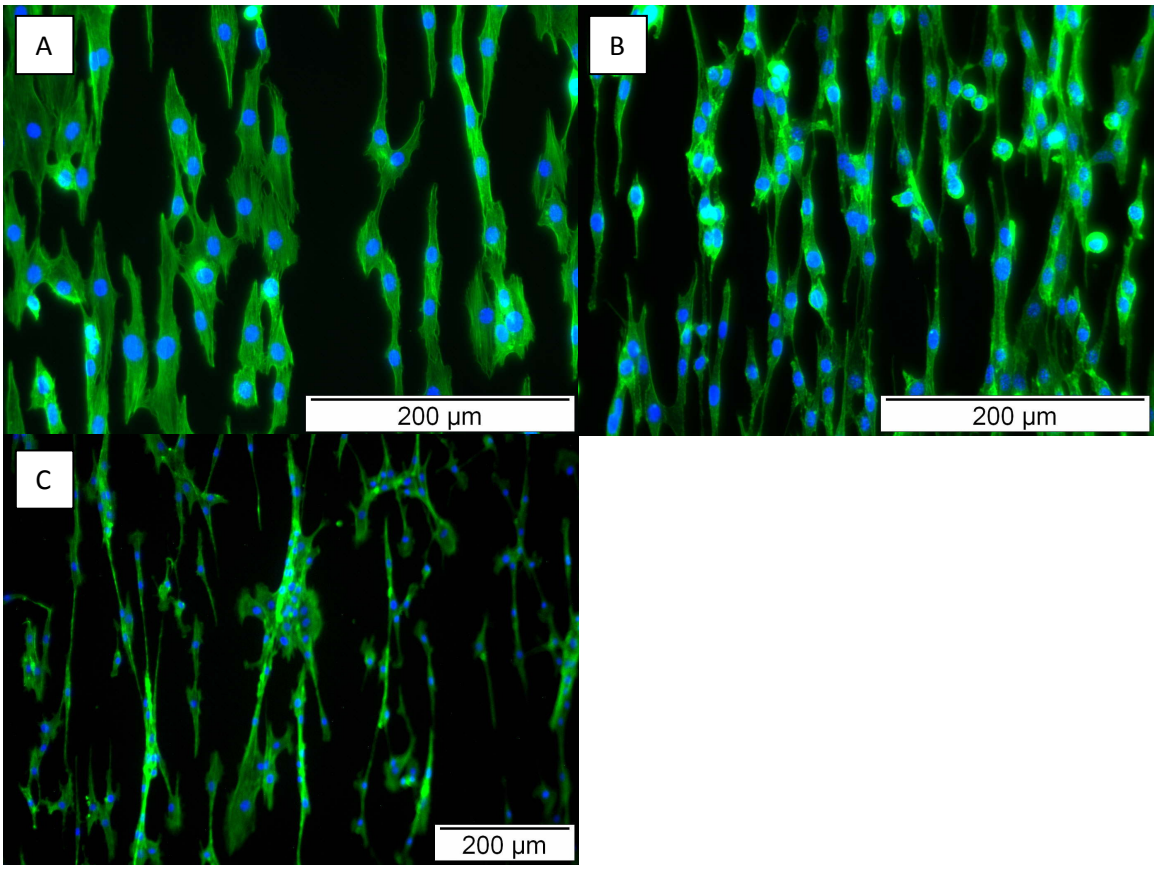

Figure 7: Fluorescence microscopy images of A) HUVECs cultured on 310 nm PDMS wrinkles and B) 510 nm PDMS wrinkles. Images taken at 20x magnification. C) RAOSMCs cultured on 310 nm PDMS wrinkles. Image captured at 10x magnification.

Since these substrates can mimic the anisotropy seen in the native heart topography, they are ideal surfaces for contact guidance studies. One application for the alignment of cells on nano-topography is cell sheeting for tissue patch and graft applications. To develop cell sheets, wrinkled microchips are coated with a thin layer of a thermo-responsive polymer called poly (N-isopropylacrylamide) (p-NIPAAM). At low temperatures (less than 32°C) the coated surface is slightly hydrophilic where cells

adhere to the surface under normal conditions. However, when the temperature increases above 37°C, the polymer surface undergoes a conformational change and becomes hydrophobic. The polymer swells and forms a hydration layer between the wrinkled surface and the cell layer, causing the cells to detach from the surface spontaneously. If a confluent layer of cells was produced on the surface beforehand, a cell sheet layer is lifted from the platform as a result [41]. The cells are typically loaded onto wrinkled chip platforms at a high seeding density so to produce a confluent layer since this layer provides close contacts of cells for enhanced communications. Once cell sheets are produced, they can be transferred onto other layers for 3D tissue patch creation or onto biodegradable materials directly for implantation [42]. As a proof of concept, the wrinkled molds previously mentioned were used to develop cell sheets of rat aortic smooth muscle cells (Figure 8). The sheets were extremely fragile and require sensitive handling to prevent folding of the sheet layer as seen in Figure 8C. Cells remained connected to one another even after sheet transfer from the wrinkled mold to a flat dish (Figure 8B).

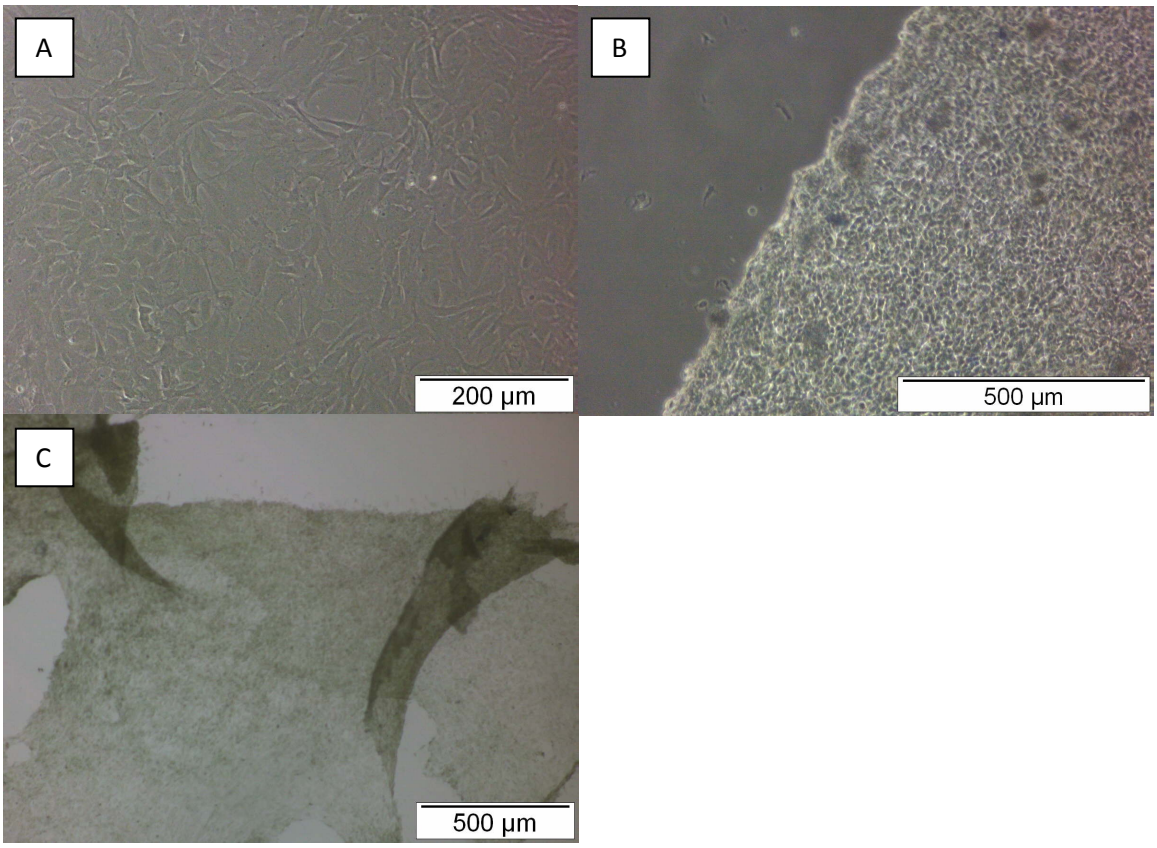

Figure 8: Optical microscopy images of cell sheeting of RAOSMCs. A) RAOSMC before lifting and B) after lifting. C) Contrast showing cell sheets folding.

2.6 Conclusions

In summary, this expedient, cost-effective method displays an impactful micro-patterning technique for cell culture analysis. While developing the 2D nano-wrinkles, the average wrinkle width increased from 310nm to 580nm as the gold sputtered coating increased from 10nm to 60nm. Furthermore, as the coating increased, the wrinkle heights also increased from 120nm to 400nm. The number of wrinkles per unit area decreased as the coating was increased and above 30nm coatings the wrinkles

began to create non-uniform wrinkling patterns which were unexpected. Nearly 100% of the cells aligned on the nano-wrinkled topography in the direction of the surface patterning, demonstrating the strong topographical influence on cell guidance.

Chapter 3: Contact Guidance on Crazed Topography

3.1 Environmental Stress Crazing

Here, we expand on the creation of multi-scale topography through solvent crazing of the PSP surface. Crazing is a localized plastic deformation process, which can lead to the fracture and failure of thermoplastic materials. Prior to failure, micro-scale topography in the form of cracks, voids, and pores are created on the polymer surface. The crazing phenomenon is generally viewed as having a negative impact on polymers since it affects structural properties, including the overall yield strength. Environmental Stress Crazing (ESCR) is known to result for up to 40% of failures in glassy thermoplastics [43] and is observed upon polymer and solvent contact. The solvent penetrates the polymer by type II diffusion processes [44] and solvent molecules reside in the interstices between chains of the polymer. If the polymer is soluble in the solvent, the polymer chains begin to coil and the bulk polymer swells due to the attractive and repulsive forces between the solvent molecules and polymer chains [45]. The solubility parameters (δ) obtained from the literature, δ = 9.9 for acetone and δ = 8.5-10.6 for polystyrene [46], show good solubility with each other, allowing the polymer matrix to swell and localized crazing to occur upon solvent absorption [47]. *Kambour et al* also obtained similar values for solubility parameters during crazing of polystyrene [48]. Moreover, as the solvent is absorbed into the amorphous regions of the polymer and the polymer continues to swell, it becomes easier for solvent to penetrate into the polymer. When the velocity of the solvent entering the polymer is faster than the ability

for the polymer to swell and expand, large internal stresses are created where the osmotic pressure induced results in cracking and small crazes at the swollen-glassy boundary [49]. Further details of environmental crazing mechanisms are discussed elsewhere [50]. Here the focus is on the morphologies and topographies atop pre-strained polystyrene by solvent crazing for contact guidance of cells. Researchers J. Chung et al., produced symmetric wrinkling patterns by swelling polystyrene with toluene [51], and C. Jacques et al. demonstrated morphologies of crazed regions of polystyrene under known tensile strains, with pore sizes from 0.1 µm to 21 µm in length as visualized below (Figure 9) [52]. Our goal was to analyze the topographies generated by the effects of solvent crazing and uniaxial strain on PSP sheets for directing cell behavior.

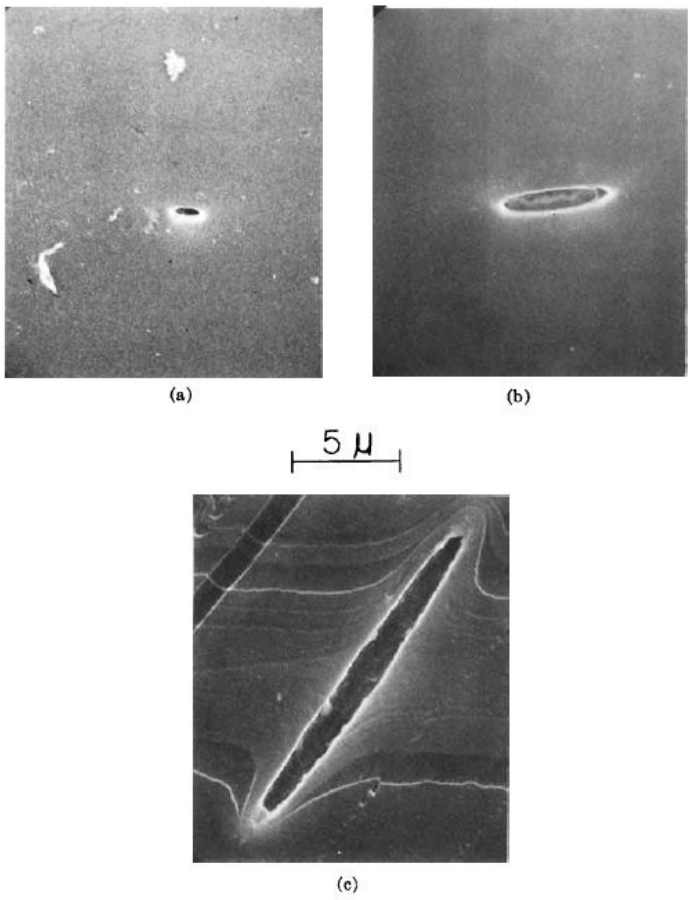

Figure 9: Scanning electron Photomicrographs on surface micropores on uniaxially oriented polystyrene films previously immersed in liquid n-hexane at 45°C (mag. 6300X): (a) 50% uniaxial elongation; (b) 100% uniaxial elongation; (c) 200% uniaxial elongation [52].

3.2 Master Mold Topography: Solvent Crazing vs. Selective Crazing

Solvent crazing can be carried out selectively on individual regions of the polymer or throughout the entire sample surface. Selective crazing can be accomplished by using instrumentation or tools to guide solvent onto specific regions of a sample. The main

issue is the amount of solvent used during selective crazing, since the solvent tends to flow and spread out quickly when in contact with the polymer surface. For example, the edge of a razor blade could be used to guide solvent in a straight line when touched lightly along the surface of a polymer. Boundary guides like the razor's edge are good for controlling the liquid flow and crazing only intended surfaces.

To achieve the crazed topography, polystyrene Shrinky Dink® sheets of 8 ½ x 11 inches (Michaels Commercial Retailer) were cut into samples of size 75 x 38 x 0.23 mm using a laser cutting and engraving unit. Samples were cut longitudinal and transverse from the original sheet as shown in Figure 10A. Each sample was washed with de-ionized (DI) water, isopropyl alcohol 99% (VWR International), rewashed in DI water, and lastly in ethanol 99% (Sigma) for ten seconds to clean the sample surface. After the ethanol treatment, cleaned samples are air dried, visually inspected for surface scratches and defects, and placed into a clean containment unit. Master mold chips were produced by solvent crazing and heat treatment. PSP samples were placed in an acetone (Sigma) bath for 10 seconds to solvent craze the surface of the sheet. Then, samples were placed in isopropyl alcohol 99% (VWR International) for 10-15 seconds to remove the acetone and were air dried at room temperature. The surface of each sample was then coated with 30nm of gold using a High-Vacuum Evaporator (Denton DV-502A).

One portion of the samples that were exposed to acetone and coated with gold as described above were then placed on top of an insulating sheet of size 75 x 38 x 1.40 mm and then on glass slides for structural support. Four small binder clips (1/4", Staples®) were used as clamping mechanisms, two on each end of the stacked layers

(left and right corners), to apply a fixed strain field and hold the sample in place (Figure 10E). The other portion of the samples were additionally processed by heat treatment in an oven (Binder FD-53) at 130°C, above T_g for polystyrene (~105°C), for four minutes to induce thermal shrinking. The temperature in the oven fluctuated by a maximum of 10°C when the door is opened for sample insertion. Samples were then removed from heat and cooled at room temperature.

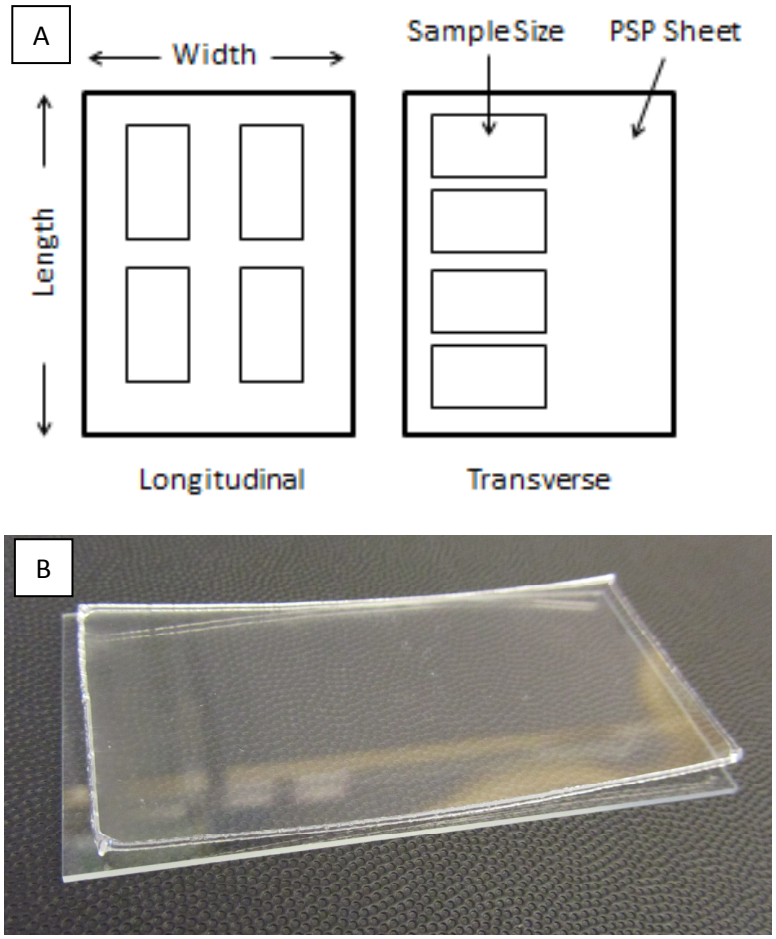


C

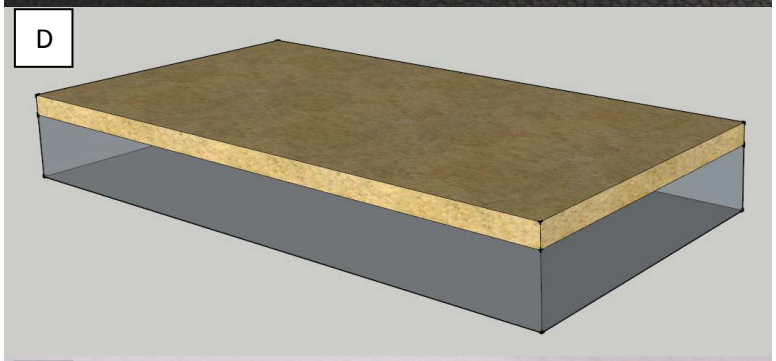
D

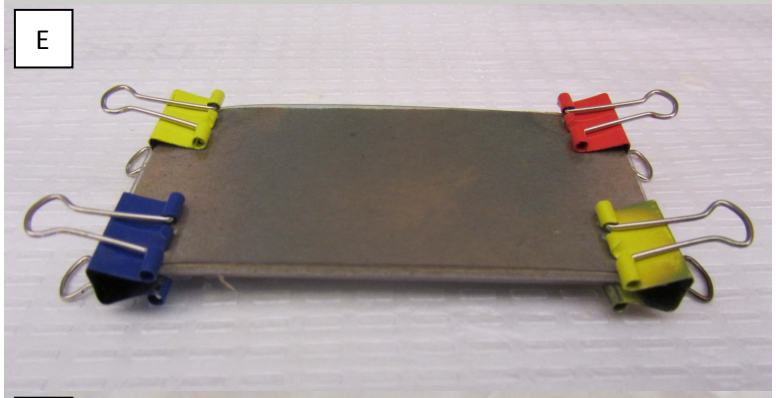
E


F

Figure 10: Description of methods for development of wrinkled and channeled platforms. A) Schematic showing cut orientation in the longitudinal and transverse directions from the original PSP sheet. B) Pre-strained polystyrene sheet on top of a glass slide for visual comparison (length = 75 mm, width = 38 mm) were cleaned with de-ionized water, isopropyl alcohol, de-ionized water, and ethanol in that order. C) Samples were then placed in acetone to induce crazing on the surface. D) Visualization of 30 nm gold coating placed on the surface of each sample. E) Gold coated samples were constrained on glass slides using binder clips and baked in an oven at 130°C for four minutes. F) The resulting shape of the PSP master mold sample having wrinkled topography after thermal treatment.

3.3 Material Characterization

PSP samples of size 6 x 6 mm were cut from the bulk sample and mounted on aluminum stubs using carbon tape and silver paint (Ted Pella, Inc.) for topographical characterization in the SEM. The SEM (FEI Quanta 200 SEM equipped with a tungsten filament) was used to obtain micrographs of the crazed structures and determine the topographical dimensions of the polystyrene surfaces. Micrographs of the surfaces on the master molds were captured at 750X magnification using a spot size of 3, a working distance of about 10 mm, and an accelerating voltage of 10 kV. AnalySIS Pro software was used to verify the width and height dimensions of the channels from the SEM micrographs.

The transparent polystyrene sheets turned opaque white within seconds of exposure to acetone. Channels and small voids were immediately formed on the surface following the solvent exposure (Figure 11). After acetone crazing, SEM images show several topographical cues on the surface of the polystyrene master molds. Features including ridges, valleys, and pores were developed on the master mold surface. Surface and cross-sectional SEM imaging showed a range in feature sizes, tabulated below in Table 2.

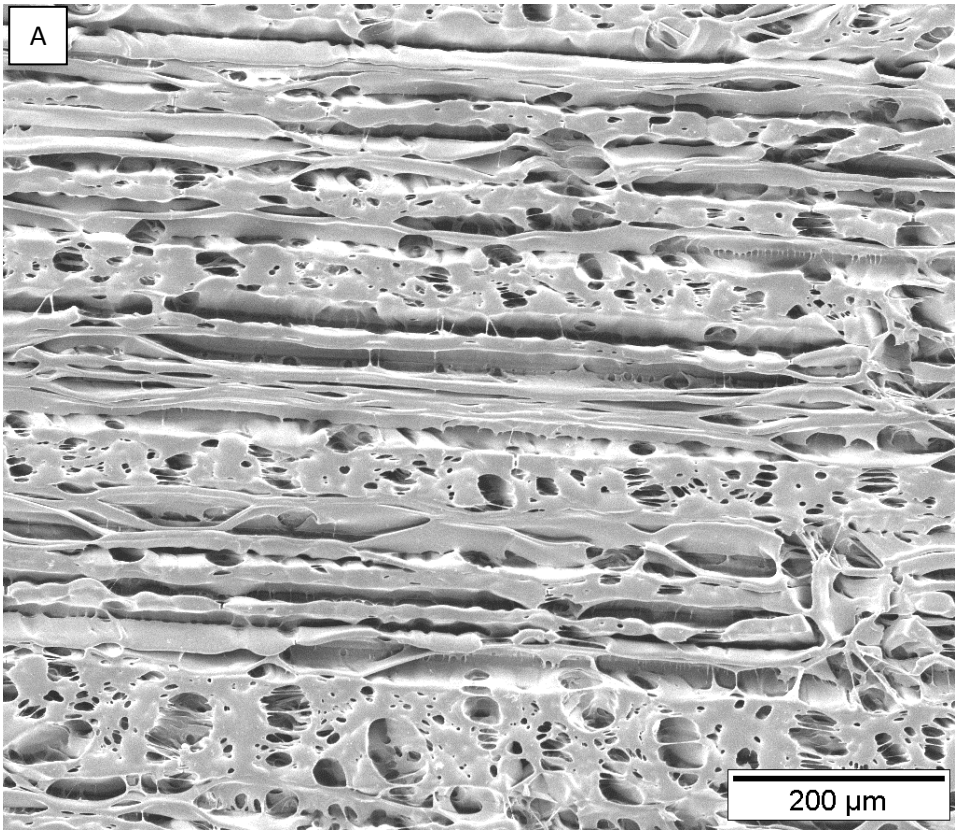

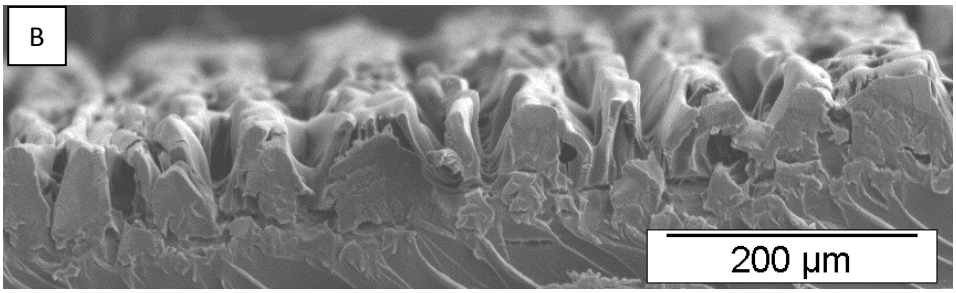

Figure 11: SEM images of acetone treated pre-stressed polystyrene (PSP) sheets. A) PSP sample cut longitudinally from the sheet. Channels and pores developed on the surface developed from surface crazing. B) Cross sectional view of (A).

It was then observed that the acetone treatment can be selectively applied to produce lines and channels along the polystyrene surface. With the help of a razorblade edge, the acetone is guided following the sharp edge, only crazing specific regions that the acetone penetrates. As seen in Figure 12 below, the width of the crazed regions is on average 10µm long. The ridge width varies depending on the distance between the prior channel produced from the blade edge and the next. In our case the ridge width was on average about 20µm long.

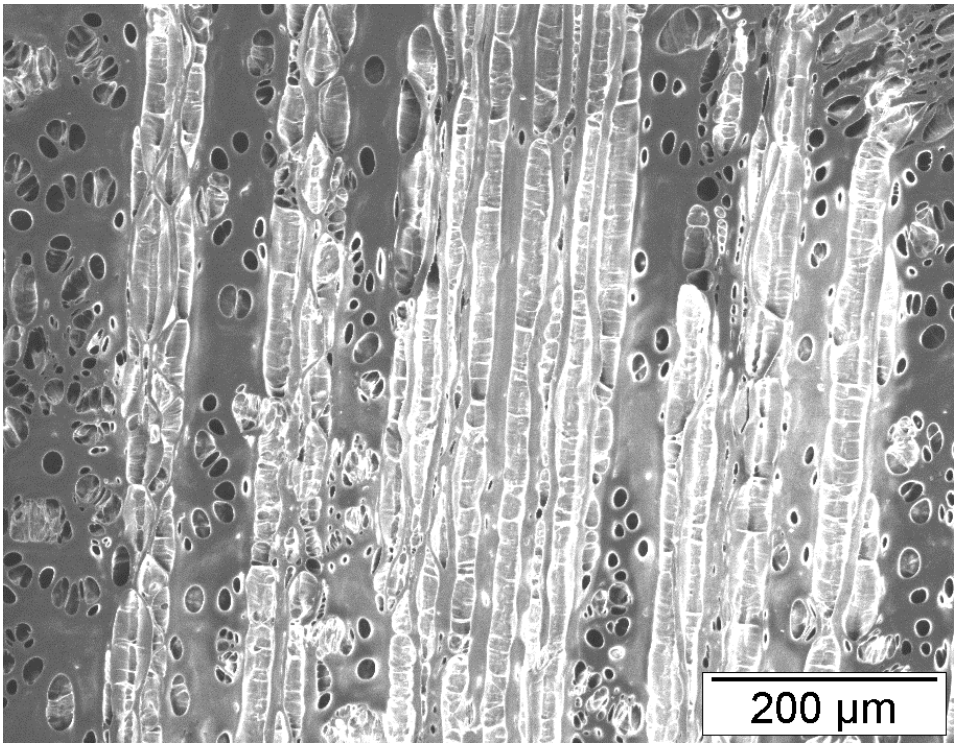

Figure 12: Selectively crazed polystyrene using an edge of a razor blade to guide the acetone liquid.

The crazed PSP molds that were shrunk in the longitudinal direction of the original polystyrene sheet were significantly different in morphology than the acetone treatment alone. Pores no longer existed on the surface, yet primary and secondary features were produced atop the master mold structures. The primary and secondary features were similar to the major and minor wavelengths seen in other literature [54]. The primary channels were uniform, aligned, and oriented in the direction of applied strain. The secondary features were oriented transverse to the strain direction, caused from the strain field produced by the mounting clips during shrinking. Longitudinally shrunk samples contained a lower number of secondary features (minor wavelengths)

throughout the bulk surface and the primary ridges were more structurally clear when compared to transverse shrunk samples (Figure 13A). Examination of the cross section showed a wrinkle depth of about 90 µm, the largest depth out of the three crazed structures, where the crazed boundary is visually apparent (see Figure 13B).

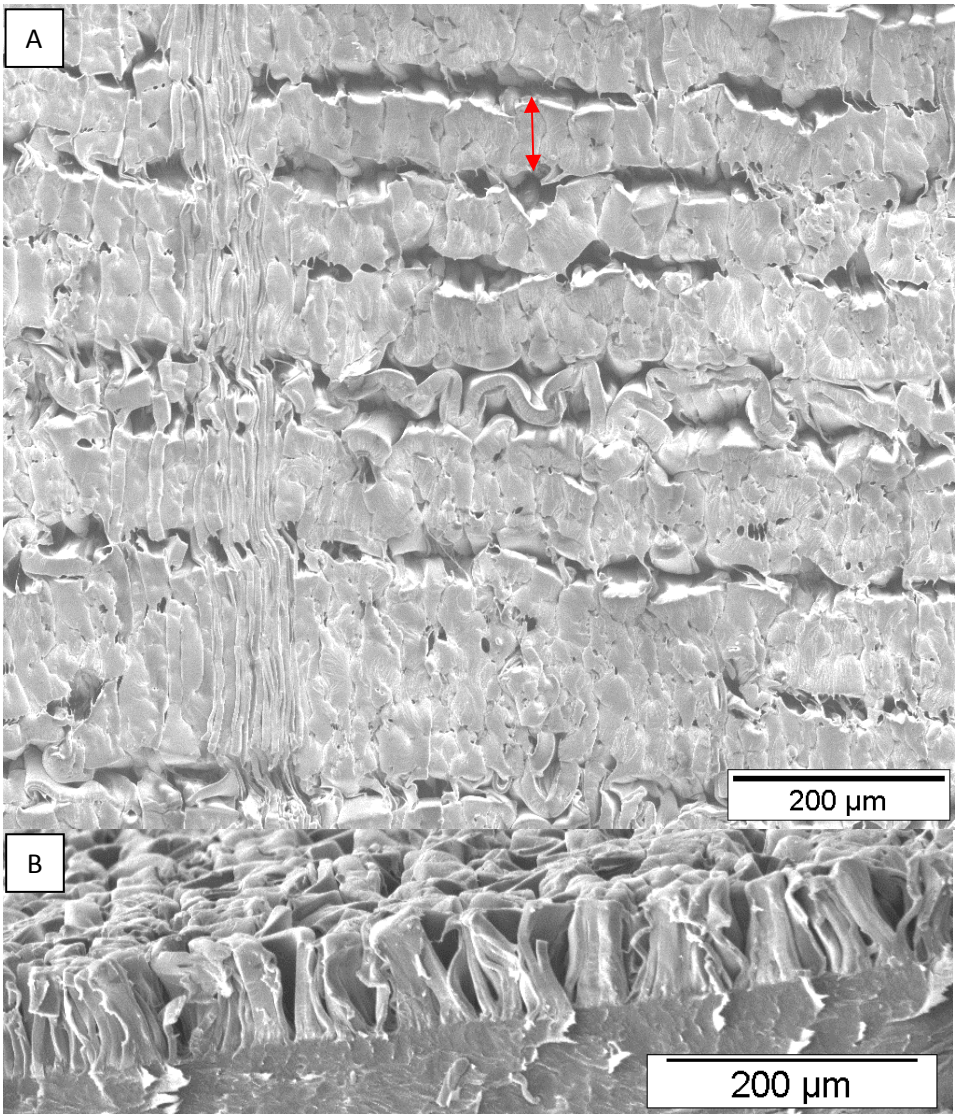

Figure 13: SEM images of shrunk-crazed longitudinal acetone treated pre-stressed polystyrene (PSP) sheets. A) PSP samples cut longitudinal to the sheet were heated at 130°C for four minutes to induce shrinking. The red arrow indicates the primary ridge width. Secondary features are oriented transverse to the primary features. B) Cross sectional view of (A).

The PSP master molds shrunk in the transverse orientation were topographically different than those shrunk longitudinally. Primary ridges were larger for transverse shrunk samples where ridge widths reached up to 97 μm in length, an increase in length of about 25 μm compared to longitudinally shrunk ridges. On the other hand, the secondary ridge distances decreased by roughly 10 μm and the secondary valleys decreased up to 8 μm in length when compared with longitudinally shrunk samples. The morphology of the secondary features atop the primary ridges are seen clearly in Figure 14, showing the anisotropic wrinkled surface topography. A cross sectional view of the master mold showed a minimum wrinkle depth of about 1 μm (in areas consisting of secondary wrinkling) and a maximum feature depth of about 65 μm throughout the entire cross section. A detailed list of the resulting dimensions from the master molds are found in Table 2 below.

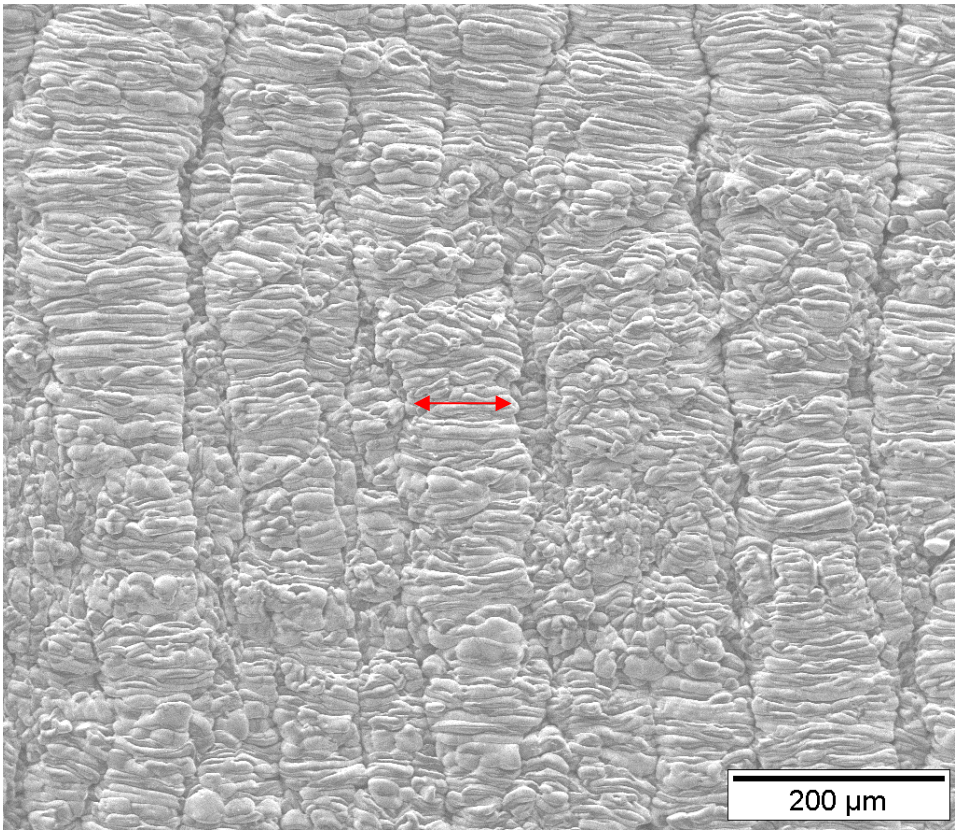

Figure 14: SEM image of shrunk-crazed transverse acetone treated pre-stressed polystyrene (PSP) sheets. PSP samples cut transverse to the sheet were heated at 130°C for four minutes to induce shrinking. Red arrow indicating the primary ridge width. Secondary features are oriented transverse to the primary features.

Seconds after exposing the PSP to acetone, the polymer swells causing a change in free volume and thus altering the refractive index for which light interacts with the material. Therefore, surface changes were noticed instantaneously and were observed by the naked eye. However, crazes, cracks, channels, and the formation of wrinkles were better analyzed through optical and electron microscopy techniques. As observed in the

acetone crazed sample, the surface topography appeared very porous after such short exposure to acetone since many holes and voids were observed. As the solvent diffuses into the glassy polymer, the polymer chains become disentangled, causing molecular conformations. Glassy polymers typically contain holes and channels on a molecular scale so the acetone molecules diffuse quicker in those regions. Since the polystyrene sheets were initially pre-strained, this process can further enhance and contribute to void formation on the molecular level, creating prime locations for solvent to penetrate and diffuse into the polymer. As the solvent escapes the polymer, the surface energy is raised and causes restrictions to molecular conformation at room temperature, thus solidifying the structure and producing the topography observed in Figure 11A. Furthermore, the cross section of the crazed substrate in Figure 11B showed a noticeable horizontal boundary apparent in the structure which indicated the penetration depth of the acetone in the ten second time period of exposure. By extending the time interval for solvent exposure it allows further diffusion of the solvent into the polymer, creating a deeper swollen-glassy boundary. Based on our observation, the topography depth can be optimized since the crazing growth rates and craze sizes are dependent upon the tensile stress in polymer structures and the time of exposure to the solvent involved [55]. This could also be a potential issue for depth accuracy since the removal of solvent from the polymer may take longer or shorter than expected. The voids and boundaries developed by crazing on the surface were forced to collide upon shrinkage of the sheet, resulting in the morphology visualized in Figure 14. Since the polystyrene sheet was originally pre-strained, its shape memory effects were

exhibited at temperatures above T_g. Upon heating to the glass transition temperature of polystyrene, both conformational and translational motion of the polymer chains allow for a partial annealing of the polymer by removal of the residual strains introduced during processing. After exposure to acetone and heat treatment, voids and channels were created on the surface up to 100 μm deep; however, the residual glassy core that was not penetrated by the solvent remains unaffected as seen in Figure 11B. Remarkably, during the heat shrinking process we observed significantly different results when strain fields were applied in both longitudinal and transverse directions to the sheet. Both sample types produced secondary wrinkling on the surface but wrinkles on the transverse oriented sheet were much smaller, almost half the width distance than the longitudinal secondary wrinkles (Figure 14). Therefore, we suspect the PSP sheets are not originally bi-axially strained simultaneously as seen in other literature [56, 57], but instead are uni-axially strained in two directions by extrusion and rolling which induces some preferred alignment of the chains due to shear flow [58]. Since the morphology of the crazes produced on the PSP follow parallel with the longitudinal direction of the sheet, we believe the strain is applied in that direction. Therefore, when shrinking crazed samples in the transverse direction, additional strain is placed on the polymer chains and the number of conformational states was ultimately reduced. As the polymer attempts to flow in directions transverse to the strain, wrinkles pile up on the surface in the attempt to heat-heal crazed regions [59]. Thus, this may be the cause of the additional formation of secondary wrinkling on the surface with ridge width distances of about 6 ± 3 μm seen in Figure 14. Secondary wrinkles may also arise from

the mismatch in stiffness between the bi-layer of gold and polymer during heat shrinking which results in wrinkles of smaller size ranges [31].

Table 2: Description of methods for sample treatment and corresponding characterization dimensions. Cell culture results indicated actin elongation and degree of alignment relative to the topography of the PDMS molds. *Vertical measurements for control sample.

Master Molds	Control	Crazed	Shrunk Crazed	Shrunk Crazed
Sample cut orientation:	Flat Control	Longitudinal	Longitudinal	Transverse
Solvent treatment:	No	Acetone	Acetone	Acetone
Heat treatment:	No	No	Yes	Yes
Primary average ridge width:	None	16 ± 10 µm	72 ± 40 µm	97 ± 39 µm
Secondary average ridge width:		None	15 ± 11 µm	6 ± 3 µm
Primary average valley width:		13 ± 7 µm	23 ± 11 µm	13 ± 10 µm
Secondary average valley width:		None	9 ± 6 µm	1 ± 0.4 µm
Primary mean ridge to ridge distance:		27 ± 10 µm	86 ± 29 µm	103 ± 38 µm
Secondary mean ridge to ridge distance:		None	13 ± 10 µm	5 ± 2 µm
Average pore diameter:		10 ± 7 µm	None	None
Average height of channel:		50 µm	90 µm	65 µm

3.4 Cell Culture Methodology

A 10:1 ratio mixture of PDMS and curing agent (Sylgard 184 Silicon Elastomer Kit; Dow Corning) was then poured on the surface of the master molds to cast the topography onto flexible, biocompatible material. The master molds, with PDMS atop, were placed in vacuum to remove air bubbles from the PDMS and then immediately placed in the oven and set to cure at 60°C for 2 hours in order for the PDMS to polymerize. Afterward, the PDMS was carefully removed from the master mold and used for biological study.

Once PDMS substrates were fabricated, cells were cultured and treated as previously explained. In short, human umbilical vein endothelial cells (HUVECs) were cultured in EGM-2 media for four days from thaw on Corning Tissue Culture 100 mm dishes coated with 0.5% gelatin. HUVECs were lifted and seeded onto PDMS substrates at a density of 30,000 cells/cm^2. HUVECs were allowed 24 hours to culture on the fabricated substrates, after which the cells were fixed with PFA and stained with Alexa Fluor 488 Phalloidin and DAPI. Afterwards, the cells were washed twice with PBS before imaging. Images were captured using a Nikon Eclipse TE2000-U fluorescence microscope and NIS-Elements AR 3.1 software. Measurements of the cell angle orientation were determined using AnalySIS Pro software.

3.5 Alignment and Orientation of Cells on Topography

PDMS molds loaded with HUVECs were analyzed after 1 day of cell culture. Cells were adherent to the PDMS substrates and aligned in the direction of the topography present

on the surface. Cells were defined as 'aligned' if their lengthwise distance was oriented within ±30° of the underlying topography direction [53]. There was a clear difference between the alignments of endothelial cells on the patterned substrates in comparison with the control PDMS chip. On the flat PDMS control sample, angle measurements were taken from the vertical axis to determine the orientation of the cells. The angle of the HUVECs orientation with respect to the vertical axis was roughly 32 ± 19° for the control sample (Table 3).

Table 3: Actin elongation and alignment angle of HUVECs on control sample and crazed PDMS molds.

PDMS molds	Control	Crazed	Shrunk-Crazed Longitudinal	Shrunk-Crazed Transverse
Average actin length relative to topography dimensions*:	51 ± 22 µm	74 ± 36 µm	75 ± 27 µm	75 ± 32 µm
Average angle of cell relative to direction of topography on platform*:	32 ± 19°	13 ± 12°	10 ± 9°	8 ± 7°

Figure 15A and 15B show no particular alignment or orientation of the cell on the flat PDMS surface. HUVECs on the acetone crazed topography extend the actin filaments roughly 23 µm in length in comparison to the flat topography (see Figures 15C and 15D). Cells were oriented at an average of about 13° with respect to the patterning direction

on the crazed surface. On the acetone crazed and shrunk longitudinal chip, cell actin filaments elongate in the lengthwise direction by 14 µm compared to the control sample and orient within 10° of the patterned surface (Figures 15E and 15F). The acetone treated and shrunk transverse molds showed alignment of the cells (Figure 15H), averaging about 8° from the topography directionality. Unaligned patterning on the bio-chips did not align the cells well, as seen on the right side in Figure 15G. HUVECs in the aligned patterning elongated to lengths of about 75 µm. Moreover, most of the cells that did align tended to reside on the ridges of the substrate rather than in the valleys (see Figure 15F).

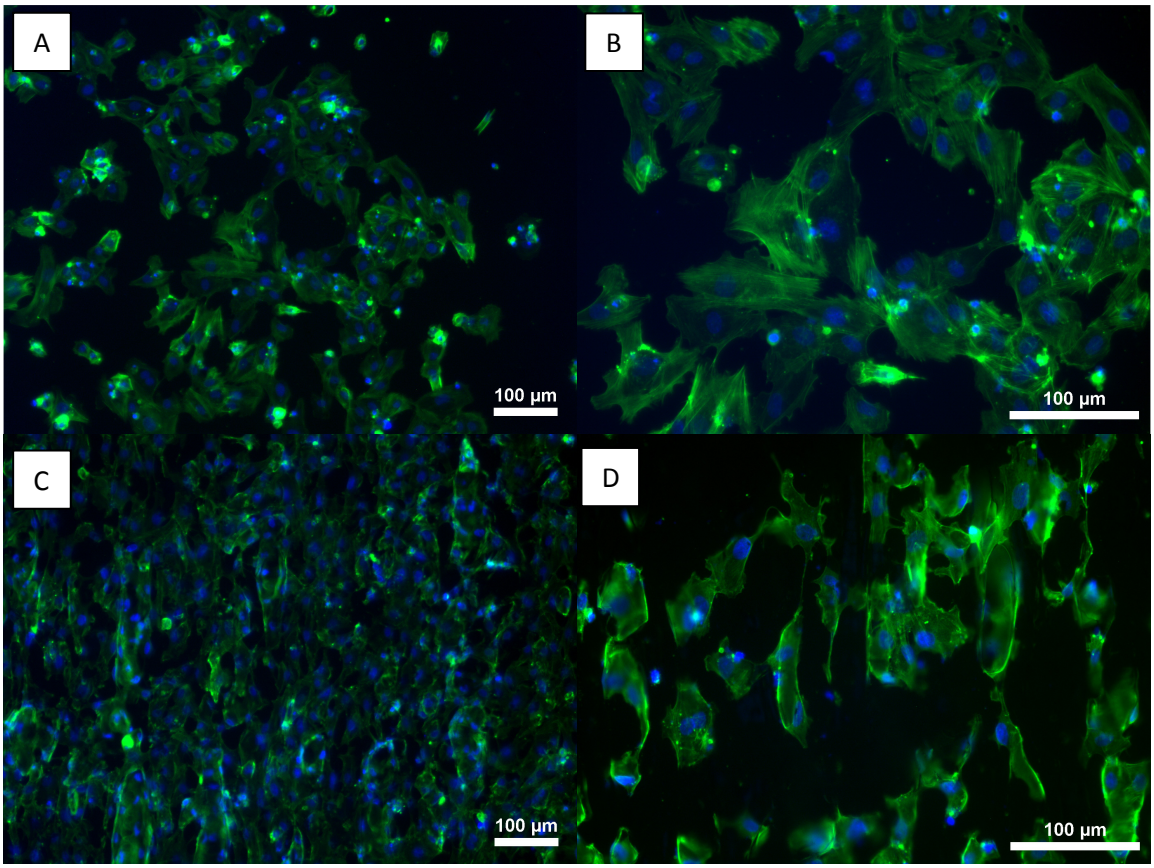

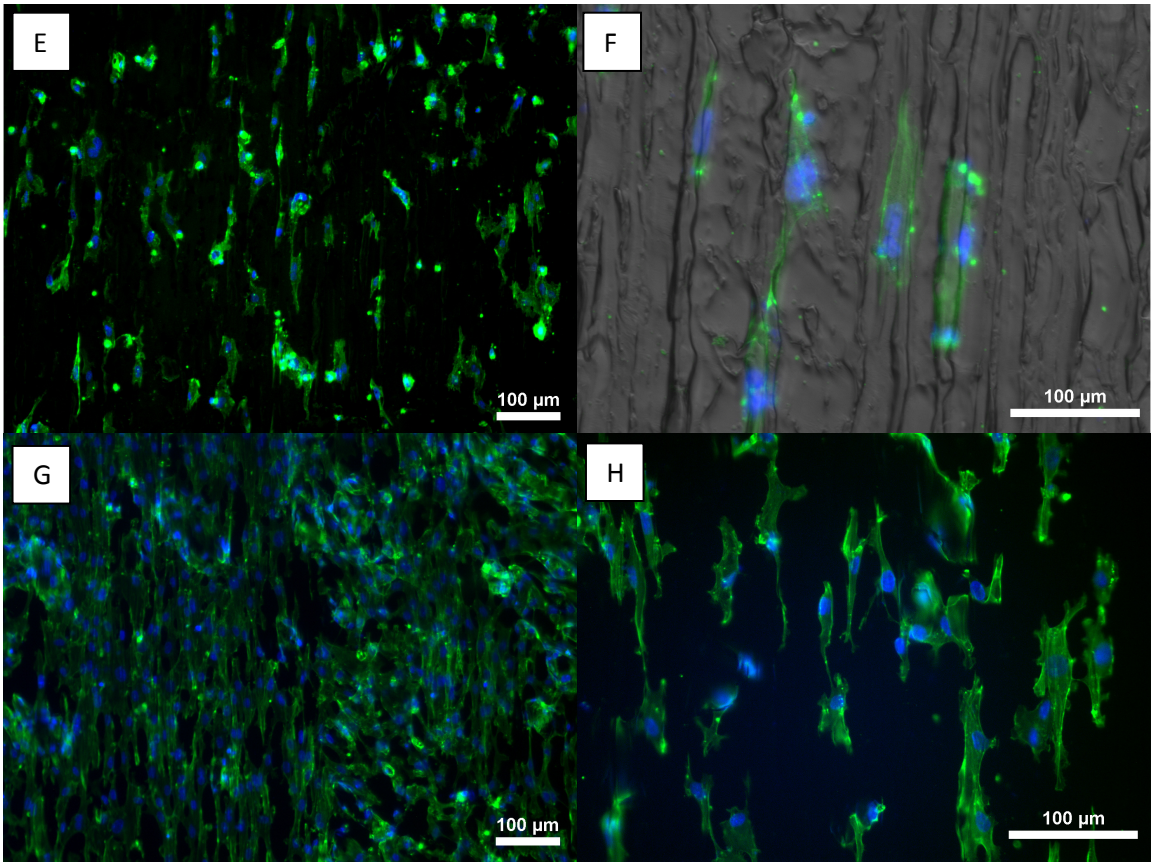

Figure 15: Human umbilical vein endothelial cells (HUVECs) stained with blue (DAPI) for nuclei and green (Alexa Fluor 488 Phalloidin) for actin filaments. Cells on a flat PDMS surface captured at low and high magnifications A) 10x and B) 20x, respectively. C) HUVECs on topography developed by acetone crazing viewed at 10x and D) 20x magnification. E) Cells on longitudinally shrunk crazed platforms at 10x and F) 20x magnification. Background lightened in (F) to show cells aligned on the ridges of the PDMS substrates. HUVECs on transverse shrunk crazed platforms at G) 10x and H) 20x magnification. Scale bar length = 100µm.

The angle of cell alignment on the PDMS control sample at about 32 ± 19° confirms that there was no specific alignment of HUVECs prior to the induced topography (see Figures 15A and 15B). Crazed topographies, however, had better alignment of cells in relation to the topographic surface direction, averaging at about 13°. Heat treating the crazed surfaces provided smaller secondary ridge widths of roughly 15 ± 11 μm and 6 ± 3 μm for longitudinal and transverse shrinking, respectively, which in turn produced smaller valleys in the PDMS molds for contact guidance experimentation. These smaller valleys in the PDMS molds provided better alignment than the crazed topographies (without heat treatment), aligning cells with an average of 8° from the topography direction. The sizes of the patterning and wrinkling could also affect cell alignment, and literature results suggest that shallow grooves below 1 μm do not orient the cells well [60]. In our observations, the size ranges developed using these methods were beneficial for alignment and elongation of cells. We also noticed some of the nuclei elongated appearing more ovular in shape and orienting themselves with the pattern direction (Figure 15H). On the other hand, some cells did not align with the topography direction, as seen in Figure 15G, since channeled structures were not well defined in all areas of the chip. HUVECs on unaligned surfaces were oriented at an average of 25 ± 18°, which is slightly more aligned than the control chip, yet does not show confluence on those surfaces. We believe the unaligned surfaces were formed from merged boundaries upon shrinkage of the PSP chip. These boundaries may not be parallel with each other during shrinking and may develop a ‘swirly’ surface where channels are curved and limited in length due to impeding boundaries. We suspect that these curved surfaces

and impeding boundaries make it difficult for the cells to elongate and align compared to the aligned patterned surfaces since there is no distinct structure for the cells to follow. We observed these 'swirly' surfaces during bi-axial shrinking of the crazed PSP [53], and as predicted, the cells did not align or follow distinct pathways (Figure 16).

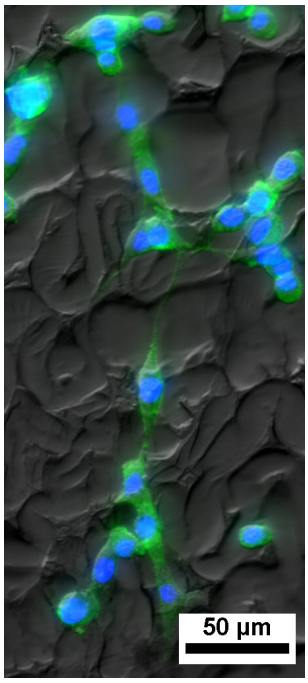

Figure 16: HUVECs atop crazed topography after bi-axial shrinking of the substrate [53].

3.6 Conclusions

In summary, resulting dimensions of the crazed PSP appeared similar to those produced by researchers A. Chen et al. [54], although these dimensions were further enhanced by providing a three-dimensional environment for cells since 2D environments do not fully represent the internal mimicry of in-vivo architecture. HUVECs were able to adhere and align on the crazed surfaces that elongated the actin filaments and oriented the cells in

the direction of the surface topography. Due to the decrease in secondary ridge width sizes, the crazed-shrunk transverse PDMS molds provided the best cell alignment out of all the crazed topographies, aligning cells with an average of 8° from the topography direction. Substrates produced by ESCR show to be beneficial to direct cellular behavior.

Chapter 4: Dynamic Rotation of Cells in Circular PDMS Microchannels

4.1 Dynamic Cell Seeding

Circular microchannels have been produced using a variety of techniques including lithography patterning [61], rod sacrificed [62], and wire sacrificed methods [63, 64]. Soft lithography methods for microchannel fabrication can vary, where in some cases rounded channels are produced by bonding two semi-circular pieces together [65] and in other cases circular channels are formed using wire- or fibers-sacrificed techniques or flowing polydimethylsiloxane (PDMS) through square channels to create round ones [66, 67]. These channels show interest to researchers for biomedical applications related to tissue engineering and vascular design. The circular channels more closely mimic in vivo systems and provide realistic morphologies for biological study.

Many researchers have shown microchannels being used for a number of applications including chaotic mixing [68], vasculature design [69], and cell culture [70]. The small sizes of channels show great use in the design and application of vascular networks to analyze cells, however, the cell-seeding procedures are inconsistent and achieving cellular confluence on a 3D surface has been known to be a challenge [71]. Current methods involve non-automated culture techniques where physical rotation of the microchannel is necessary to achieve confluence on all surfaces [72]. These methods are inconsistent from user to user and the physical rotation itself is a tedious process. Since cells are fragile and physical manipulation of the construct can be a primary cause of cell

death, current techniques remain an issue for 3D cell seeding. Alternatively, rotating vessels and hybridization ovens have been used to dynamically control the seeding and culture process [73], however, the speeds of rotation are typically no slower than 5 rpm and can cause cell death due to shear stresses inside the channels. To address this issue, a custom device is built to dynamically rotate microchanneled constructs at slow speeds using a hands-free approach.

4.2 Formation of Circular PDMS Microchannels

Circular microchannels are formed by casting thin metal wire of 1mm diameter in a 10:1 ratio mixture of PDMS and curing agent (Sylgard 184 Silicon Elastomer Kit; Dow Corning) (Figure 17). The PDMS polymerizes after 2 hours in an oven (Binder FD-53) at 60C. The PDMS molds are then placed in ethanol 99% (Sigma) to soak for 1 hour. The PDMS molds are then removed from ethanol and air dried for 5 minutes. The metal wire can now easily be removed using tweezers or clamping tools without damaging the internal surface of the channels [74]. PDMS constructs are then placed in a UV-ozone treatment for 30 minutes to change the surface properties of the PDMS from hydrophobic to hydrophilic.

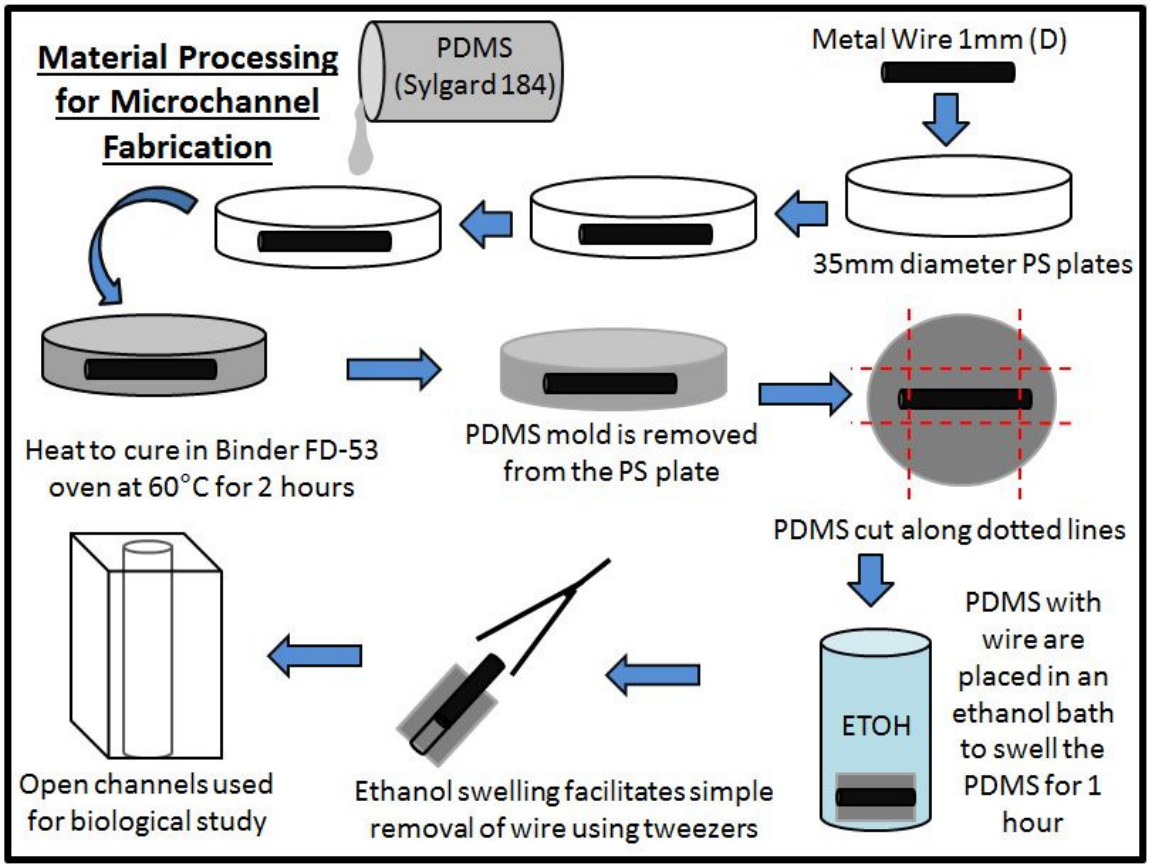

Figure 17: Schematic of material processing for development of microchannels.

A 10:1 ratio mixture of PDMS and curing agent (Sylgard 184 Silicon Elastomer Kit; Dow Corning) is poured into 35mm polystyrene (PS) tissue culture (TC) plates with metal wire strands (1mm diameter) to cast the shape of the wire. TC Plates were heated to 60°C for 2 hours to cure the PDMS. The samples were cut to expose both ends of the wire inside the PDMS and immediately placed into an ethanol bath for one hour to help facilitate removal of the wire mold. After swelling of the PDMS, wires were removed using tweezers and the resulting channels were used for biological study.

Human umbilical venous endothelial cells (HUVECs) and Rat aortic smooth muscle cells (RAOSMCs) were cultured in media for four days from thaw on Corning Tissue Culture 100 mm dishes coated with 0.5% gelatin (Figure 18). A gelatin coating was placed inside the channels and allowed to sit for 1 hour prior to cell seeding. The cells were lifted and replated into gel coated fabricated PDMS constructs at a concentration of 32,000 cells/µl.

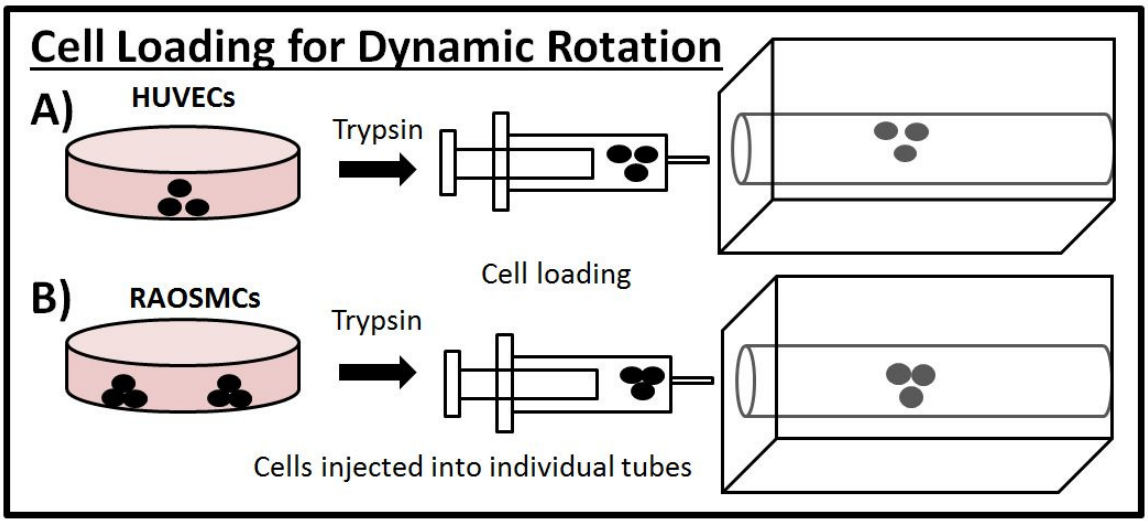

Figure 18: Diagram of cell loading for dynamic rotation for both A) Human umbilical venous endothelial cells (HUVECs) and B) Rat aortic smooth muscle cells (RAOSMCs).

The PDMS constructs are placed in a glass vial filled with media nutrients and attached to the dynamic rotation device. Cells were cultured in a dynamic rotation device for at least 2 days to ensure cell adhesion to the construct. Upon removal, cells were fixed with 4% paraformaldehyde (PFA), and then washed twice with Phosphate Buffer Solution (PBS). Blocking and permeablization solution consisting of 3ml of 1ng/ml

Bovine Serum Albumen (Sigma) (BSA) in PBS, 150ul of Donkey Serum, and 21ul of TritinX-100 was then loaded into the microchannels and allowed to sit for 30 minutes. For staining, 5 µl of Alexa Fluor 488 Phalloidin (Invitrogen) and 50 µL of 2 ng/mL DAPI (CalBiochem) were added to the blocking and permeablization solution and flushed through the channels at a rate of 2 ml per hour using a pump flow controller (New Era Pump Systems, Inc). Samples were kept in the dark during staining for 1 hour by placing a dark container over the pump flow controller. Microchannels were washed with PBS prior to imaging. Images were captured using a Nikon Eclipse TE2000-U fluorescence microscope and analyzed using NIS-Elements AR 3.1 software.

4.3 Dynamic Rotation Device

A dynamic rotation device was built using several components (Figure 19). A 12V direct current (DC) (EDACPOWER) power supply was hooked up to an ATX pin controller to give an output of 3V. The lead wires were then secured to a potentiometer to lower the voltage output to as low as 1.5V. The power source was connected to a motorized gear box setup consisting of a K'NEX motor kit (3V motor, 1:553.3) and a 6-speed gearbox (TAMIYA). The speed at the end of the K'NEX motor kit can be controlled down to 1 rotation every 14 seconds. The gear box enabled an output ratio of 1300.9:1, so that the output speed is reduced to approximately 0.7 rotations per hour. The device and its components were placed into an incubator and the PDMS construct in the glass vial is secured to the output gear shaft. After extended periods of dynamic rotation, the device is turned off and the PDMS constructs are carefully removed from the vial.

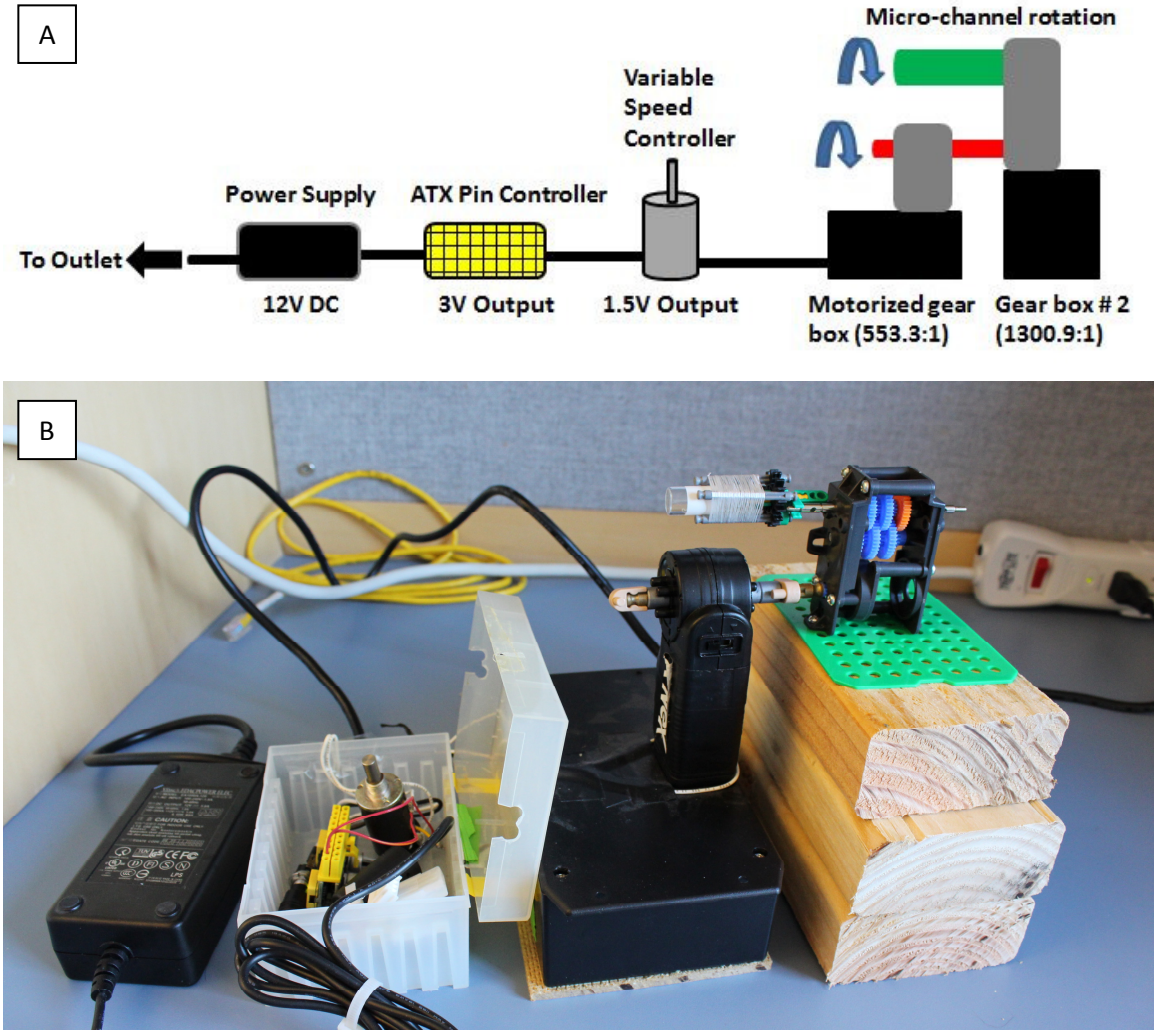

Figure 19: A) Diagram and B) Picture of dynamic rotation device setup.

4.4 Biological Impact

Human venous endothelial cells (HUVECs) and Rat aortic smooth muscle cells (RAOSMCs) were used in the dynamic rotation experiment in PDMS microchannels. Both

HUVECs and RAOSMCs were grown on standard flat bottom tissue culture (TC) plates (Figure 20).

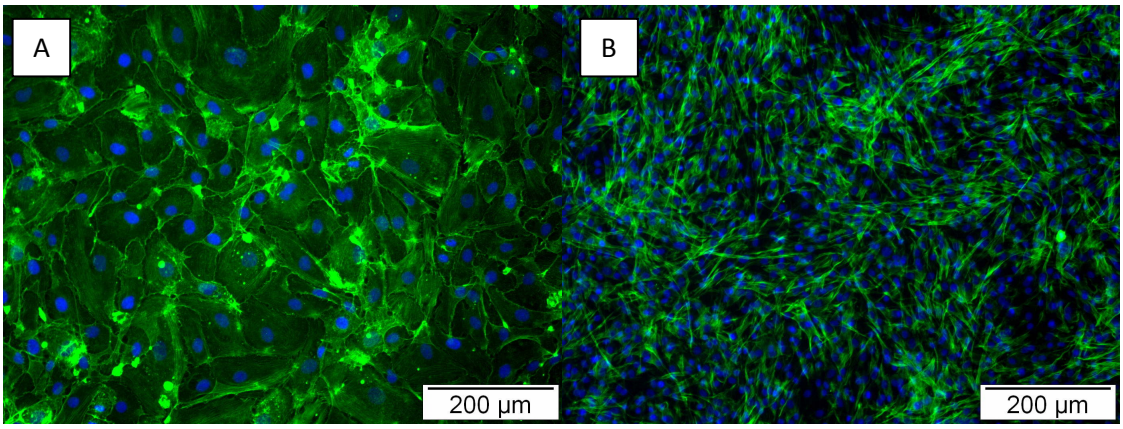

Figure 20: A) Fluorescence microscopy image of HUVECs on flat bottom TC plate. B) Fluorescence microscopy image of RAOSMCs on flat bottom TC plate.

Individual cell types were cultured in PDMS microchanneled structures for 2 days in dynamic rotation. The tubular PDMS structures maintained their shape throughout the culture period. Cells were loaded into the constructs at low concentrations for proof-of-concept. At day 2, the cells were adhered to the circumference of the tubes and began to develop cell-to-cell connections. Figure 21 shows HUVECs that were identified using DAPI as a nuclear stain (blue) and Alexa Fluor 488 Phalloidin as an actin filament stain (green) (Figure 21).

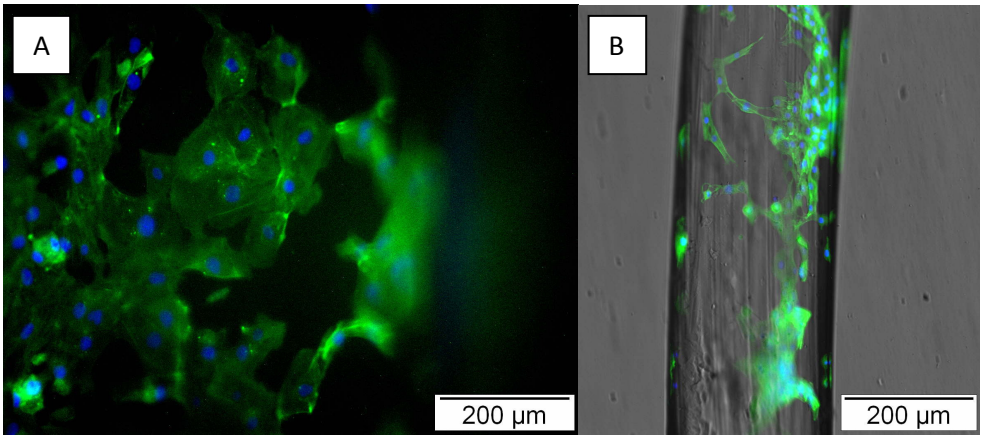

Figure 21: Fluorescence microscopy images of A) HUVECs located on the inside the 1mm diameter PDMS channel after 4 days of dynamic rotation. The blurred region on right indicates curvature of the channel wall. B) RAOSMCs adhere to the inner walls of a 250µm diameter channel.

Once viability of the cells was confirmed after multiple days in dynamic culture, the cells were then loaded at a seeding density of 30,000 cells/cm^2 into the tubular constructs. At day 2 in culture, RAOSMCs achieved a semi-confluent layer around the inner circumference of the tube. Optical images show numerous cell-to-cell connections were formed in the microchannels. Very few cells were washed out during staining procedures, which was a good indicator for strong adherence to the tubes. The cells can be seen adhering to the side walls of the tube and become visibly blurred in the curvature of the channel (Figure 22).

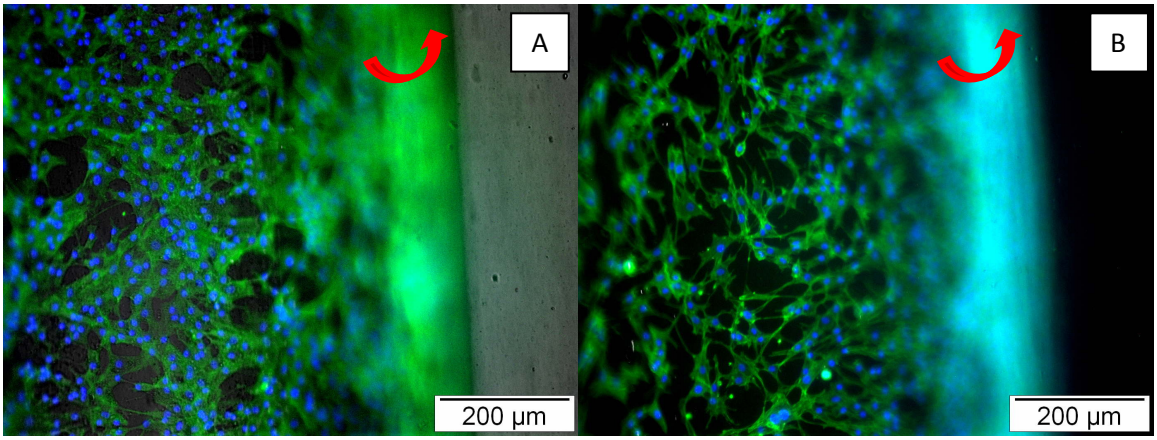

Figure 22: RAOSMCs loaded into constructs at a concentration of 32,000 cells/µl. Fluorescence microscopy images taken A) with and B) without the surface background. Semi-confluent layers produced after 2 days in culture. Red arrows indicating the curvature of the channel edge.

A cell count confirmed that the number of cells in the tubes increased by as much as 480% over the culture period, creating semi-confluent layers of cells (Figure 22A). Cell density increased from the seeding amount of approximately 30,000 cells/cm^2 up to 156,000 cells/cm^2 at day 2 in culture. The increase in the number of cells was unexpected since many of the initial challenges involved issues with cells adhering to the polymer. If the UVO methodology was not properly applied to the PDMS, then hydrophobic groups would exist on the surface and prevent cell adhesion to the construct. Additionally, issues remained involving the fixing and staining procedures, which may have flushed a number of cells out of the tubes. The flow rate controller helped control the variability of flow rates, at a constant 2 ml per hour, compared to pipetting techniques. In addition, when the experiment would run longer than two days,

the old culture media was replaced daily thereafter with new media to ensure cells received fresh nutrients and oxygen in the tube passage. Adding new media causes a temporary discontinuity of rotation for cells in the tubes and also requires the tube to be flushed of waste media, which may contribute to the detachment of cells in the PDMS channels. Therefore, future designs may provide a rotational inlet-outlet valve to conduct media transfers without interrupting the rotation process.

4.5 Conclusions

The wire-sacrificed technique was an effective fabrication method for the design and formation of circular, seamless microchannels in PDMS. The dynamic rotation of microchannels provided favorable culture conditions and caused endothelial and smooth muscle cell types to adhere to the inner circumference of the PDMS microchannels, creating a three-dimensional connection of cells. Confluent layers were produced inside the channels by increasing the cell count during cell seeding. The dynamic rotation speed was controlled by optimization of variable resistors and gear-boxes to achieve a rotation speed of 1 rotation per hour. In future experiments, we suspect that increasing the rotation speed will prevent cell-surface connections and prevent confluence as the adherence decreases. Additionally, other research studies may explore a bi-layer of cells inside the microchannels to properly mimic in vivo vasculature. A layer of smooth muscle cells might first be used on the channel surface, and later adding endothelial cells atop of the previous cell layer. We expect there to be significant challenges in this approach due to the compatibility of each cell type under

dynamic conditions. Cell loading techniques may prove to be challenging as well in this approach since many of the cells can be pushed to the surrounding media due to shear forces during seeding. As a future study, researchers could consider the use of bio-degradable materials such as poly- (glycerol sebacate) (PGS) for implantable applications of vascular structures *in-vivo*. Furthermore, new processing techniques using 3D printing may show possibilities to rapidly create master-mold substrates that may, in-turn, provide further benefit to unique tissue engineering applications.

Chapter 5: Future Directions

5.1 Multi-scale Topography

One future direction for this research is using a multi-scale device composed of both nanowrinkles and crazed topography on the same bio-chip as seen in Figure 23. Depending on the cell types and function, this design may prove to be beneficial for enhanced cell connections in some cases. Furthermore, crazed micro-topography shows great promise in the fields of tissue and bio-engineering studies. In particular, based on the topography of crazed surfaces, these lab-on-a-chip platforms may be ideal for heart and liver patch repair work [19] and also demonstrate promising use for microfluidic and channel flow applications [75].

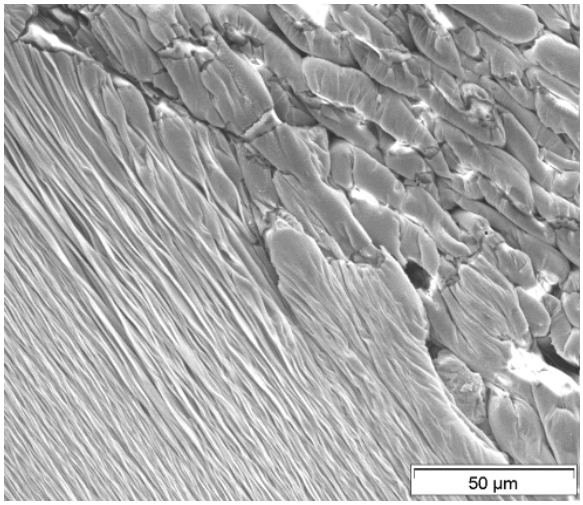

Figure 23: SEM micrograph of multi-scale topography - acetone treatment and non-acetone treated wrinkles on a single bio-chip.

5.2 Topography from Natural Materials

Another future direction for this research is analyzing cell guidance on natural materials with anisotropic topography. Many ECM based topographies are mimicked by electrospinning silk-based materials which can provide anisotropic patterning on small-scales [29].

There are, however, materials with directional surface patterning that are found in nature, like the Echinocactus grusonii spine. Since the cactus spine is a material from nature, they are a renewable resource which can be harvested and serve as master molds for cell guidance studies. There are a number of potential benefits to using natural materials for cell guidance studies, including but not limited to, rapid fabrication processing, cost efficient, bio-degradable and/or eco-friendly, reproducible, and robust molds. As a proof of concept, endothelial cells were cultured on the molded surface topography of the Echinocactus grusonii spine for contact guidance.

Spines were gathered from the Echinocactus grusonii plant and were immediately washed with deionized water and 70% ethanol (Sigma). The spine surface structure was imaged using scanning electron microscopy. Spines were molded in PDMS and soft-molds were prepared for biological study as explained in previous chapters. HUVECs were cultured and plated as explained previously for wrinkled substrates. Cells were imaged at 10x magnification using a Nikon Eclipse Ti confocal microscope with a D_Eclipse C1 camera setup.

The Echinocactus grusonii spine topography is similar in morphology to the topography generated previously using wrinkling techniques on pre-strained polystyrene. However, the size features are slightly larger on the cactus spine compared to the PSP wrinkles.

The SEM was used to analyze surface features and cross-sectional views of the spines. The width of the entire spine was typically between 800um to 1000um in length as shown by the red arrow in Figure 24B. The distance between the midpoints of the valleys was approximately 10um and was classified as the wrinkle width (Figure 24C). The length of each valley was approximately 1-3um in length. The depth of the wrinkles on average was approximately 10um. The cross sectional SEM image shows the boundary between the exterior surface and interior layer (Figure 24D).

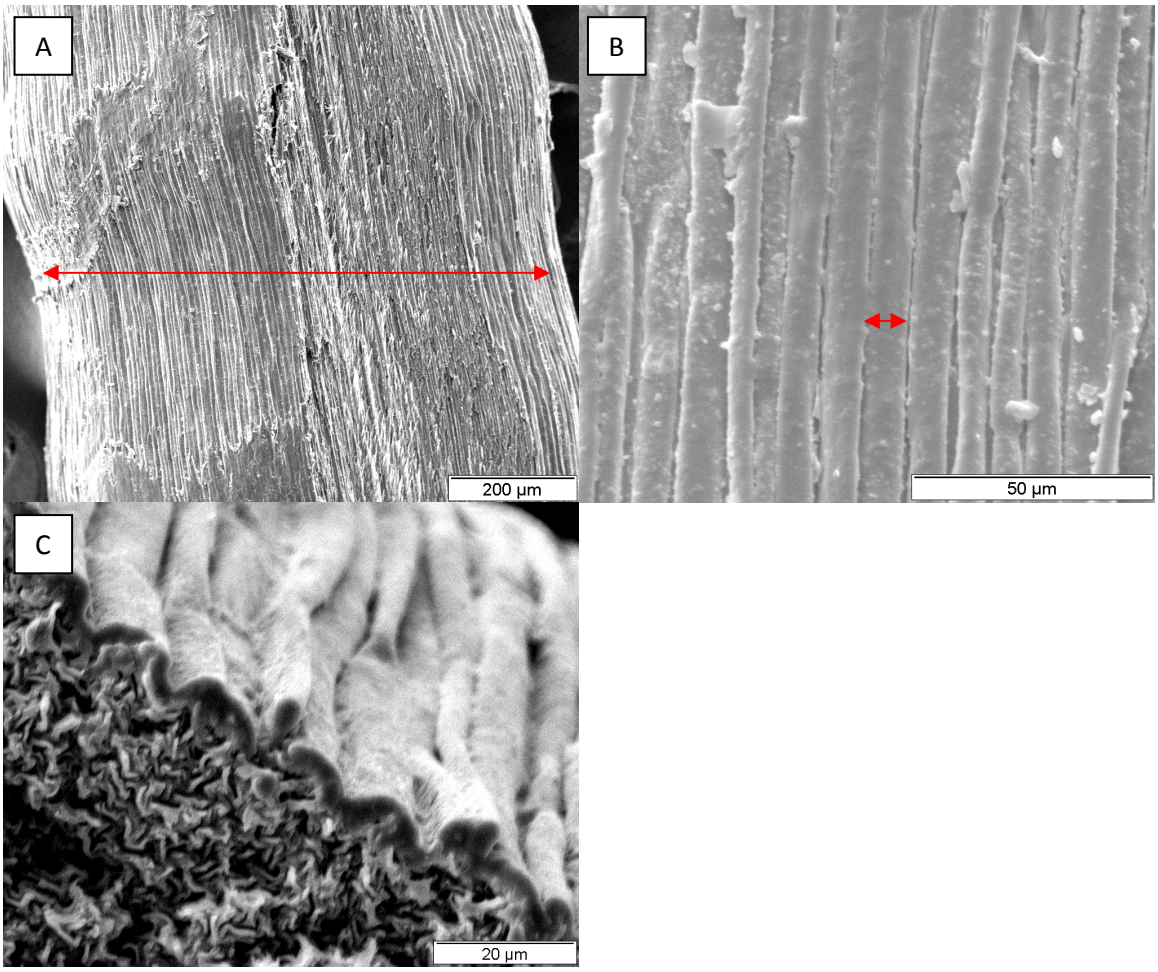

Figure 24: SEM images of the *Echinocactus grusonii* spine surface taken at A) 50X and B) 200X magnifications. Red arrow in (A) indicating the width of the cactus spine and in (B) indicating the wrinkle width. C) Cross-sectional image of the cactus spine edge.

Cells were cultured on the cactus wrinkle molds for 24 hours prior to staining and imaging. Cells on the flat control PDMS surface were comparable to the control samples for prior studies. To ensure the alignment of the cells was not contributed to a possible chemical reaction from the cactus plant, a control sample was generated by gently rubbing the spines on a flat PDMS surface prior to culture. There was no observable

difference between this control and the flat PDMS control, suggesting that the topography was the key component to cell elongation. HUVECs elongated their actin filaments on the cactus mold topography as visualized in Figure 25.

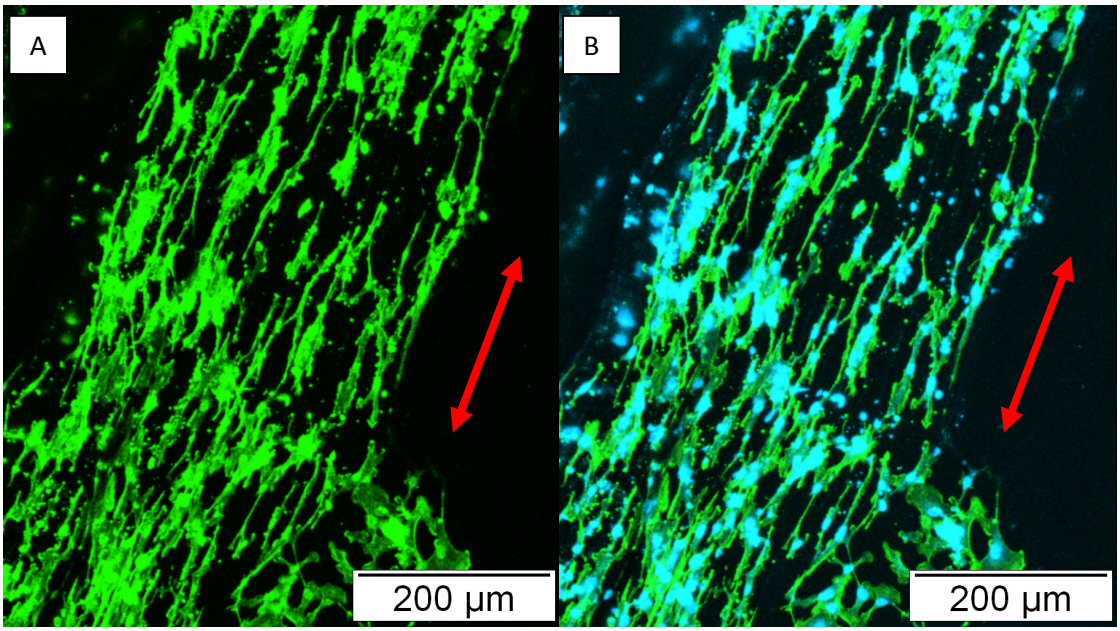

Figure 25: Confocal images of HUVECs on cactus topography stained for A) actin filaments (green) and B) overlay of actin (green) and nucleus (blue). Red arrows indicating anisotropic topography direction.

The cactus surface topography interestingly showed to be beneficial to align HUVECs even though the scale of the topography was much larger compared to the nanowrinkles produced from the polymer wrinkling methodology. This result reiterates the impact of alternative cost-effective devices for biomedical applications. From our observations and results, we expect these mold-structures could similarly be used for cell-sheeting applications as observed previously. Through modification of the PDMS

molds, the cactus surfaces may also have potential use in vascular designs and microfluidics, while encouraging new applications for natural materials.

References

[1] L. R. Madden, D. J. Mortisen, E. M. Sussman, S. K. Dupras, J. Fugate, J. L. Cuy, & B. D. Ratner, Proangiogenic scaffolds as functional templates for cardiac tissue engineering. Proceedings of the National Academy of Sciences of the United States of America, 2010, 107, 15211–15216.

[2] B. N. Brown, C. Barnes, R. T. Kasick, R. Michel, T. W. Gilbert, D. Beer-Stolz, & S. F. Badylak, Surface characterization of extracellular matrix scaffolds. Biomaterials, 2010, 31, 428–437.

[3] R. O. Hynes, The extracellular matrix: not just pretty fibrils. Science, 2009, 326, 1216–1219.

[4] G. A. Abrams, S. L. Goodman, P. F. Nealey, M. Franco, & C. J. Murphy, Nanoscale topography of the basement membrane underlying the corneal epithelium of the rhesus macaque. Cell and tissue research, 2000, 1, 39–46.

[5] K. E. Mccloskey, Emerging Trends in Cell and Gene Therapy. M. K. Danquah & R. I. Mahato, Eds., 2013, 471–483.

[6] D. Kim, P. Provenzano, C. Smith, & A. Levchenko, Matrix nanotopography as a regulator of cell function, The Journal of cell biology, 2012, 3, 351–360.

[7] E. K. F. Yim, K. W. Leong, Significance of synthetic nanostructures in dictating cellular response. Nanomedicine : nanotechnology, biology, and medicine, 2005, 1, 10–21.

[8] P. Clark, P. Connolly, A.S. Curtis, J.A. Dow, & C.D. Wilkinson, Topographical control of cell behaviour - I. Simple step cues, Development (Cambridge, England), 1987, 99, 439-448.

[9] S. Britland, H. Morgan, B. Wojiak-Stodart, M. Riehle, A. Curtis, & C. Wilkinson, Synergistic and hierarchical adhesive and topographic guidance of BHK cells, Experimental cell research, 1996, 2, 313–325.

[10] G. Jr, M. Cheng, C.J. Bettinger, T. Jeffrey, R. Langer, & L.E. Freed, Accordion-like honeycombs for tissue engineering of cardiac anisotropy, Nature Materials, 2009, 12, 1003–1010.

[11] N. Li, A. Tourovskaia, & A. Folch, Biology on a chip: microfabrication for studying the behavior of cultured cells, Critical reviews in biomedical engineering, 2003, 31, 423–488.

[12] E. Sţepień, J. Stanisz, & W. Korohoda, Contact guidance of chick embryo neurons on single scratches in glass and on underlying aligned human skin fibroblast, Cell biology international, 1999, 23, 105–116.

[13] S. Biela, Y. Su, J.P. Spatz, & R. Kemkemer, Different sensitivity of human endothelial cells, smooth muscle cells and fibroblasts to topography in the nano-micro range, Acta biomaterialia, 2009, 5, 2460–2466.

[14] E. Yim, R. Reano, S. Pang, A. Yee, C. Chen, & K. Leong, Nanopattern-induced changes in morphology and motility of smooth muscle cells, Biomaterials, 2005, 26, 5405–5413.

[15] A. Teixeira, G. Abrams, P. Bertics, C. Murphy, & P. Nealey, Epithelial contact guidance on well-defined micro- and nanostructured substrates, Journal of cell science, 2003, 116, 1881–1892.

[16] P. Uttayarat, G. K. Toworfe, F. Dietrich, P. I. Lelkes, & R. J. Composto, Topographic guidance of endothelial cells on silicone surfaces with micro- to nanogrooves: orientation of actin filaments and focal adhesions, Journal of biomedical materials research, 2005, 75, 668–680.

[17] S. Masuda, T. Shimizu, M. Yamato, & T. Okano, Cell sheet engineering for heart tissue repair, Advanced drug delivery reviews, 2008, 60, 277–285.

[18] M. R. Williamson, R. Black, & C. Kielty, PCL-PU composite vascular scaffold production for vascular tissue engineering: attachment, proliferation and bioactivity of human vascular endothelial cells, Biomaterials, 2006, 27, 3608–3616.

[19] W. S. Turner, X. Wang, S. Johnson, C. Medberry, J. Mendez, S. F. Badylak, K. E. McCloskey, Cardiac tissue development for delivery of embryonic stem cell-derived endothelial and cardiac cells in natural matrices, Journal of biomedical materials research. Part B, Applied biomaterials, 2012, 100, 2060-2072.

[20] A. S. G. Curtis, & C. D. W. Wilkinson, Reactions of cells to topography, Journal of Biomaterials Science Polymer Edition, 1998, 9, 1313–1329.

[21] E. Martínez, E. Engel, J. Planell, & J. Samitier, Effects of artificial micro- and nano-structured surfaces on cell behaviour, Annals of anatomy, 2009, 191, 126–135.

[22] Y. S. Choi, L. G. Vincent, A. R. Lee, K. C. Kretchmer, S. Chirasatitsin, M. K. Dobke, & A. J. Engler, The alignment and fusion assembly of adipose-derived stem cells on mechanically patterned matrices, Biomaterials, 2012, 33, 6943–6951.

[23] K. Efimenko, W. E. Wallace, & J. Genzer, Surface Modification of Sylgard-184 Poly(dimethyl siloxane) Networks by Ultraviolet and Ultraviolet/Ozone Treatment. Journal of Colloid and Interface Science, 2002, 2, 306–315.

[24] J. El-Ali, P. K. Sorger, & K. F. Jensen, Cells on chips, Nature, 2006, 442, 403–411.

[25] N. Bursac, Cardiomyocyte Cultures With Controlled Macroscopic Anisotropy: A Model for Functional Electrophysiological Studies of Cardiac Muscle, Circulation Research, 2002, 91, 45–54.

[26] N. Geisse, S. P. Sheehy, & K. K. Parker, Control of myocyte remodeling in vitro with engineered substrates, In vitro cellular & developmental biology, 2009, 45, 343–350.

[27] M. Wood, Colloidal lithography and current fabrication techniques producing in-plane nanotopography for biological applications, Journal of the Royal Society, 2007 4, 1–17.

[28] W. Y. Yeong, H. Yu, K. P. Lim, K. L. G. Ng, Y. C. F. Boey, V. S. Subbu, & L. P. Tan, Multiscale topological guidance for cell alignment via direct laser writing on biodegradable polymer, Tissue engineering Part C - Methods, 2010, 16, 1011–1021.

[29] X. Zong, H. Bien, C. Y. Chung, L. Yin, D. Fang, B. S. Hsiao, & E. Entcheva, Electrospun fine-textured scaffolds for heart tissue constructs, Biomaterials, 2005, 26, 5330–5338.

[30] P. Y. Wang, J. Yu, J. H. Lin, & W. B. Tsai, Modulation of alignment, elongation and contraction of cardiomyocytes through a combination of nanotopography and rigidity of substrates, Acta biomaterialia, 2011, 7, 3285–3293.

[31] C. Fu, A. Grimes, M. Long, C. G. L. Ferri, B. D. Rich, S. Ghosh, & M. Khine, Tunable Nanowrinkles on Shape Memory Polymer Sheets, Advanced Materials, 2009, 21, 4472-4476.

[32] B. Wójciak-Stothard, A. Curtis, W. Monaghan, K. MacDonald, & C. Wilkinson, Guidance and activation of murine macrophages by nanometric scale topography, Experimental cell research, 1996, 223, 426–435.

[33] X. Zhao, Y. Xia, & G. M. Whitesides, Soft lithographic methods for nano-fabrication, Journal of Materials Chemistry, 1997, 7, 1069–1074.

[34] J. I. Luna, J. Ciriza, M. E. Garcia-Ojeda, M. Kong, A. Herren, D. K. Lieu, & K. E. McCloskey, Multiscale biomimetic topography for the alignment of neonatal and embryonic stem cell-derived heart cells, Tissue engineering. Part C, Methods, 2011, 17, 579-588.

[35] M. Behl, & A. Lendlein, Shape memory polymers, Materialstoday, 2007, 10, 20–28.

[36] A. Lendlein, & S. Kelch, Shape-memory polymers, Angewandte Chemie, 2002, 41, 2034-2057.

[37] D. Nguyen, S. Sa, J. D. Pegan, B. Rich, G. Xiang, K. E. McCloskey, & M. Khine, Tunable shrink-induced honeycomb microwell arrays for uniform embryoid bodies, Lab on a chip, 2009, 9, 3338–3344.

[38] A. Chen, D. K. Lieu, L. Freschauf, V. Lew, H. Sharma, J. Wang, & M. Khine, Shrink-film configurable multiscale wrinkles for functional alignment of human embryonic stem cells and their cardiac derivatives, Advanced materials, 2011, 23, 5785–5791.

[39] E. Cerda, & L. Mahadevan, Geometry and Physics of Wrinkling. Physical Review Letters, 2003, 90, 074302.

[40] G. Velve-Casquillas, M. Le Berre, M. Piel, & P. T. Tran, Microfluidic tools for cell biological research. Nano today, 2010, 5, 28–47.

[41] J. Yang, M. Yamato, C. Kohno, A. Nishimoto, H. Sekine, F. Fukai, & T. Okano, Cell sheet engineering: recreating tissues without biodegradable scaffolds. Biomaterials, 2005, 26, 6415–6422.

[42] W. S. Turner, X. Wang, S. Johnson, C. Medberry, J. Mendez, S. F. Badylak, & K. E. McCloskey, Cardiac tissue development for delivery of embryonic stem cell-derived endothelial and cardiac cells in natural matrices. Journal of biomedical materials research. Part B, Applied biomaterials, 2012, 100, 2060-2072.

[43] J. C. Arnold, Environmental stress crack initiation in glassy polymers, Trends in polymer science, 1996, 4, 403-408.

[44] D. De Kee, Q. Liu, & J. Hinestroza, Viscoelastic (Non-Fickian) Diffusion, The Canadian Journal of Chemical Engineering, 2008, 83, 913–929.

[45] M. Mukherjee, A. Singh, J. Daillant, A. Menelle, F. Cousin, C. E. A. Saclay, & L. L. Brillouin, Effect of Solvent-Polymer Interaction in Swelling Dynamics of Ultrathin Polyacrylamide Films : A Neutron and X-ray Reflectivity Study, Macromolecules, 2007, 40, 1073–1080.

[46] A. Barton, Solubility Paramaters, Chemical Reviews, 1975, 75, 731-753.

[47] G. A. Bernier & R. P. Kambour, The role of organic agents in the stress crazing and cracking of poly(2,6-dimethyl-1,4-phenylene oxide), Macromolecules, 1968, 1, 393-400.

[48] R. P. Kambour, C. L. Gruner, & E. E. Romagosa, Solvent crazing of “dry” polystyrene and “dry” crazing of plasticized polystyrene, Journal of Polymer Science: Polymer Physics Edition, 1973, 11, 1879–1890.

[49] L. M. Robeson, Environmental Stress Cracking: A Review, Polymer Engineering and Science, 2012, 1-15.

[50] E. H. Andrews, G. M. Levy, & J. Willis, Environmental crazing in a glassy polymer: the role of solvent absorption, Journal of Materials Science, 1973, 8, 1000–1008.

[51] J. Y. Chung, A. J. Nolte, & C. M. Stafford, Diffusion-Controlled, Self-Organized Growth of Symmetric Wrinkling Patterns, Advanced Materials, 2009, 21, 1358–1362.

[52] C. H. M. Jacques, H. B. Hopfenberg, V. Stannett, & N. Carolina, The Effect of Orientation on the Morphology and Kinetics of Solvent Crazing in Polystyrene, Journal of Applied Polymer Science, 1974, 18, 223–233.

[53] R. Hatano, K. Mercurio, J. I. Luna, D. E. Glaser, V. J. Leppert, & K. E. McCloskey, Endothelial cells derived from embryonic stem cells respond to cues from topographical surface patterns, Journal of biological engineering, 2013, 7, 1-12.

[54] A. Chen, D. K. Lieu, L. Freschauf, V. Lew, H. Sharma, J. Wang, & M. Khine, Shrink-film configurable multiscale wrinkles for functional alignment of human embryonic stem cells and their cardiac derivatives, Advanced materials, 2011, 23, 5785–5791.

[55] K. Jakus, J. E. Riiter, & C. A. Larsen, Crazing and Acoustic Emission in Poly(Methyl Methacry1ate)/Acetone and Polystyrene/Methanol Systems, Polymer Engineering and Science, 1981, 21, 854-858.

[56] P. Rizzo, & A. R. Albunia, Syndiotactic Polystyrene Films : Orientation and Structural Changes Upon Biaxial Drawing, Macromolecular Chemistry and Physics, 2011, 212, 1419–1426.

[57] A. Ajji, & X. Zhang, Correlations between orientation and some properties of polymer films and sheets, Journal of Plastic Film and Sheeting, 2002, 18, 105-116.

[58] A. Peterlin, Drawing and extrusion of semi-crystalline polymers, Colloid & Polymer Science, 1987, 265, 357-382.

[59] O. K. Spurr, & W. D. Niegisch, Stress crazing of some amorphous thermoplastics, Journal of Applied Polymer Science, 1962, 6, 585-599.

[60] A. Curtis, & C. Wilkinson, Topographical control of cells, Biomaterials, 1997, 18, 1573-1583.

[61] Z. Huang, X. Li, M. Martins-Green, & Y. Liu, Microfabrication of cylindrical microfluidic channel networks for microvascular research. Biomedical microdevices, 2012, 14, 873–883.

[62] H. Perry, C. Greiner, I. Georgakoudi, M. Cronin-Golomb, & F. G. Omenetto, Simple fabrication technique for rapid prototyping of seamless cylindrical microchannels in polymer substrates. The Review of scientific instruments, 2007, 78, 044302.

[63] S.-H. Song, C.-K. Lee, T.-J. Kim, I. Shin, S.-C. Jun, & H.-I. Jung, A rapid and simple fabrication method for 3-dimensional circular microfluidic channel using metal wire removal process. Microfluidics and Nanofluidics, 2010, 9, 533–540.

[64] Y. Jia, J. Jiang, X. Ma, Y. Li, H. Huang, K. Cai, & Y. Wu, PDMS microchannel fabrication technique based on microwire-molding. Chinese Science Bulletin, 2008, 53, 3928–3936.

[65] M. Ville, P. Coquet, P. Brunet, & R. Boukherroub, Simple and low-cost fabrication of PDMS microfluidic round channels by surface-wetting parameters optimization. Microfluidics and Nanofluidics, 2011, 12, 953–961.

[66] X. Yang, O. Forouzan, J. M. Burns, & S. S. Shevkoplyas, Traffic of leukocytes in microfluidic channels with rectangular and rounded cross-sections. Lab on a chip, 2011, 11, 3231–3240.

[67] M. Abdelgawad, C. Wu, W.-Y. Chien, W. R. Geddie, M. Jewett, & Y. Sun, A fast and simple method to fabricate circular microchannels in polydimethylsiloxane (PDMS). Lab on a chip, 2011, 11, 545–551.

[68] A. D. Stroock, S. K. W. Dertinger, A. Ajdari, I. Mezic, H. Stone, & G. M. Whitesides, Chaotic mixer for microchannels. Science, 2002, 295, 647–651.

[69] L. K. Fiddes, N. Raz, S. Srigunapalan, E. Tumarkan, C. Simmons, A. R. Wheeler, & E. Kumacheva, A circular cross-section PDMS microfluidics system for replication of cardiovascular flow conditions. Biomaterials, 2010, 31, 3459–3464.

[70] E. Leclerc, Y. Sakai, & T. Fujii, Cell Culture in 3-Dimensional Microfluidic Structure of PDMS, Biomedical Microdevices, 2003, 5, 109–114.

[71] G. Villalona, B. Udelsman, D. R. Duncan, E. McGillicuddy, R. F. Sawh-Martinez, N. Hibino, & C. K. Breuer, Cell-seeding techniques in vascular tissue engineering. Tissue engineering. Part B, Reviews, 2010, 16, 341–350.

[72] S. Editors, S. Bhatia, C. Chen, M. T. Group, & C. Stark, Endothelialized Networks with a Vascular Geometry in Microfabricated Poly (dimethyl siloxane), Biomedical Microdevices, 2004, 6, 269–278.

[73] B. Nasseri, I. Pomerantseva, M. R. Kaazempur-Mofrad, F. W. H. Sutherland, T. Perry, E. Ochoa, & J. P. Vacanti, Dynamic rotational seeding and cell culture system for vascular tube formation. Tissue engineering, 2003, 9, 291–299.

[74] A. Morarka, S. Agrawal, S. Kale, A. Kale, S. Ogale, K. Paknikar, & D. Bodas, Quantum dot based immunosensor using 3D circular microchannels fabricated in PDMS. Biosensors & bioelectronics, 2011, 26, 3050–3053.

[75] G. M. Whitesides, The origins and the future of microfluidics, Nature, 2006, 442, 368–373.